Geochronology, Geochemistry and Petrology of Neoproterozoic Granitoids and Sediments from the SMGC, India; Eastern India's role in the final amalgamation of Gondwana.

Thesis submitted in accordance with the requirements of the University of Adelaide for an Honours Degree in Geology

Anthony Rees

November 2015

THE UNIVERSITY of ADELAIDE

TITLE: GEOCHRONOLOGY, GEOCHEMISTRY AND PETROLOGY OF NEOPROTEROZOIC GRANITOIDS AND SEDIMENTS FROM THE SMGC, INDIA; EASTERN INDIA'S ROLE IN THE FINAL AMALGAMATION OF GONDWANA.

RUNNING TITLE: GEOCHRONOLOGY, GEOCHEMISTRY AND PETROLOGY OF NEOPROTEROZOIC GRANITOIDS AND SEDIMENTS FROM THE SMGC, INDIA

ABSTRACT

According to the Gondwana reconstructions, Western Australia lay next to the Shillong Plateau in north eastern India. The Neoproterozoic metasedimentary rocks known as the Shillong Group may represent the deposits of a sedimentary basin that lay between India and Australia before the formation of Gondwana. The aim of this study is to investigate the tectonic evolution of the India-Australia collision as Gondwana formed by constraining the age and provenience of the Shillong Group and the petrogenesis of the igneous intrusions found within it. U-Pb ICPMS zircon data from the metasediments show they have a maximum depositional age of 978.4±26.69Ma, and contain dominate age populations of ca. 1150, ca. 1180Ma and ca. 1750Ma. The crosscutting igneous rocks were dated as 522±19Ma and were found to have geochemical signatures of magmatic arc rocks. These data have been interpreted as evidence that suggest that India collided with Gondwana during the Cambrian, marking the completion of the supercontinent Gondwana.

KEYWORDS

Gondwana, India, Pinjarra Orogeny, Meghalaya, Shillong Plateau

TABLE OF CONTENTS

LIST OF FIGURES AND TABLES

INTRODUCTION

The Shillong Meghalaya Gneissic Complex (SMGC) is thought of by many workers as a location in which the Pinjarra Orogen can be found exposed (Kelsey et al., 2008; Collins is Pisarevsky, 2005; Fitzsimmons 2000) and yet is thought to be poorly constrained (Collins and Pisarevsky, 2005). The region is thought to be a NE-SW trending intracratonic basin (Nandy, 2001), filled with Proterozoic metasediments known as the Shillong group and intruded by Neoproterozoic to Cambrian intrusives thought to be the result of a magmatic arc (Ghosh 2005; Yin et al 2010). Workers such as Yin et al., (2010) and Santosh (2005) have suggested that this magmatic arc is the result of the subduction of the Australian/Mawson Plate underneath India during the final formation of Gondwana. If this is the case, it supports the hypothesis that the Pinjarra Orogen represents the closure of a Neoproterozoic ocean (Fitzsimons, 2000; Collins 2003), along which the separate Neoproterozoic continents of India and Australia collided, marking the completion of Gondwana (Collins and Pisarevsky, 2005; Meert 2003; Collins, 2003).

In this paper the tectonic evolution of the India-Australia collision as Gondwana formed is investigated. The age and provenience of the Shillong Group is constrained the along with the petrogenesis of the igneous intrusions found within it. This is achieved using XRF and LA ICPMS geochemical analysis, U/Pb geochronology via LA ICMPS along with petrological analysis. The interpretations brought forth in this paper are made with the hope of further containing and supporting existing hypotheses to further the collective understanding of this fascinating area.

GEOLOGICAL SETTING

The Shillong Plateau is east-west trending horst block in north eastern India in the state of Meghalaya (Ghosh, 2005). The region comprises of the Garo, Khasi, and Jaintia hills in the west, north, and south respectively. The region has an average elevation of 1000m (Kayal, 2008), however, can reach up to 1,961m at the Shillong Peak. The region is the north eastern portion of the Indian Shield and is separated from the terrains of Bangladesh by the Dauki Fault and from the Peninsular India by the Rajmahal-Garo gap (Ghosh, 2005).

The region has been a focus of large-scale uplift through the Mesozoic to Quaternary and is suggested to have caused the Indian plate to contract to 4±2mm/y over the last 2 – 5 million years (Bilham and England, 2001). Bilham and England (2001) purposed a geological model for the region, describing it as a "pop-up" structure. The Shillong Plateau is bounded by thrust faults, the Dauki and the Oldham fault, from which either compressional or flexural forces elevate the plateau. Bilham and England (2001) also used this as evidence to suggest that the Dauki and Oldham faults penetrate the entire crust.

The lithology of the Shillong Plateau can be broken into 5 different units, which will be discussed here, note these descriptions are taken from Yin et al., 2010:

- The Mainly Eocene Strata: This unit sits stratigraphically above the Shillong Group and include; coal bearing sandstone, mudstone and shale.
- Cretaceous Strata (both sedimentary and ingenious): This unit comprises of siltstone, mudstone thickly bedded basalt and sandstone.
- The Proterozoic Shillong Group: The Shillong group is of Proterozoic age, with dominate ages at ca. 900, ca. 1250Ma and ca. 1750Ma (Yin et al 2010)

and consists of mudstone, phyllite, siltstone and course grained, cross bedded arenite. This unit is stratigraphically above the Precambrian crystalline basement and is intruded by the Proterozoic granites. The contact between the Shillong Group and the Precambrian Crystalline Basement is an isoclinally folded phyllite, where the cleavage has transposed the protolithic bedding

- Proterozoic granites: The Granites are broken into 2 different kinds of granite, Gr-1, which is a biotite bearing granite with mafic lenses ca. 30 – 50cm long and 10 – 20 cm wide and Gr-2, a K-feldspar bearing granite. Gr-1 has been intruded by both deformed and undeformed dykes and veins and has been dated using U/Pb dating at 1100Ma (Yin et al 2010). Gr-2 was also dated using U/Pb dating and was dated to be 520Ma – 480 Ma (Yin et al 2010).
- Precambrian Crystalline Basement Rocks: These rocks form the basement to the Shillong Plateau and consist of amphibolite, garnet schist, quartzo-feldspathic gneiss and orthogneiss. As with the Proterozoic Shillong Group, the basement has been intruded by large deformed granitoids. At the contact with the Shillong Group, highly altered schist is found (Yin et al 2010).

The metasedimentary rocks of the Shillong Group are the dominant rock type in the Shillong Plateau and fill a NE-SW trending intracratonic basin (Nandy, 2001). These metasediments were metamorphosed to greenschist facies (Nandy, 2001) and are in direct contact with the Precambrian crystalline basement rocks, where the contact was defined by an isoclinally folded phyllite (Yin et al., 2010). The basement is metamorphosed to granulite facies in areas, especially in the central regions around

Sonapahar (Ghosh et al, 2005). A series of basic eruptives known as the Khasi Greenstone appears both discordantly and concordantly (Mazumder, 1986) while syn- to late-tectonic igneous bodies crosscut the Shillong Group metasediments (Ghosh et al., 2005).

In this study, the age of detrital zircons from the Shillong Group was determined to constrain the maximum depositional age and explore the provenance of the protoliths. In addition, the chemistry and wage of the Gr-2 granitoids were examined. Taken together these data were used to better understand the tectonic evolution of the region

The amalgamation of eastern Gondwana

Gondwana was thought to have come together by the amalgamation of two large continents, East Gondwana and West Gondwana, with the site of the collision being the East African Orogen (McWilliams, 1981) that lay to the west of India in Gondwana. In the 2000's a number of workers suggested that the Pinjarra Orogen (that separates Australia from India in Gondwana) was not an intracontinental orogen, as had been previously thought, but represented the closure of a Neoproterozoic ocean (Fitzsimons, 2000; Collins 2003). In this model, East Gondwana did not exist as a Neoproterozoic continent, instead India and Australia formed separate Neoproterozoic continents and collided along the Pinjarra Orogen (Collins and Pisarevsky, 2005; Meert 2003). Since then, the Pinjarra Orogen has been suggested to be found exposed in the Leeuwin Block of far SW Australia (Collins 2003), in Antarctica (Kelsey et al., 2008), the Naturaliste Plateau (Halpin et al., 2008) and in NE India (Yin et al., 2010; Santosh 2005).

Previous work done on the Pinjarra Orogeny and North Eastern India

A number of ages have been put forward for the Pinjarra orogeny, this is not only due to the varying techniques used, but also because the ages are derived from different geographical locations which may represent different stages of the orogen. Kelsey et al (2008), in their work on metamorphism in Prydz Bay, Antarctica concluded that the area was involved in the Pinjarra Orogen and used U/Pb dating techniques to conclude the orogenesis there occurred between ca. 570 -500 Ma. The Naturaliste Plateau, which is off the coast of Western Australia was interpreted to be associated with The Leeuwin Complex, and therefore the Pinjarra orogen and was dated using electron microprobe chemical dating of monazite to reveal an age of ca. 515 Ma (Halpin et al., 2008). The Leeuwin Complex, Western Australia has also been dated; Collins (2003) used U-Pb dating via the Sensitive High-mass Resolution Ion Microprobe (SHRIMP), to get dates of 522 ± 5 Ma (Collins 2003). Shillong Plateau has been dated by Yin et al., (2010) who conducted a study were 5 igneous rocks were dated using U/Pb via ion microprobe where they found ages between ca. 520 – 430Ma. Ghosh et al. (2005), who has also worked in the Meghalaya, found ages between 479Ma and 550Ma

METHODS

U/Pb Geochronology

The analytical methods used for U/Pb dating follow those of Payne et al. (2006). Samples were collected by hand using the geological map presented in a paper by Yin et al., (2010). Samples designated for geochronology were cut using a rock saw and broken down into pebble size using a jaw crusher. Samples were then ground down incrementally using a disk crusher, to its minimum setting of roughly 1 to ½ a

millimetre. After which the particles of rock were sorted between two sieves at 79nm and 400nm grade. The 79 – 400nm portion was collected and separated via panning, conventional magnet techniques, Frantz isodynamic separation (at 0.6nT) and heavy liquids (methylene iodide). After which they were handpicked, mounted on epoxy resin blocks and carbon coated.

The aforementioned mounts were imaged using the CL on a Phillips XL-20 SEM with attached Gatan Cathode Luminescence (CL) in order to identify zoning in the zircons. The carbon coating was removed before the U/Pb isotopic analysis was undertaken on the NewWave 213 nm Nd-YAG laser in a He ablation atmosphere, coupled to an Agilent 7500cs ICP-MS at the University of Adelaide. A spot size of 30um, frequency of 5 Hz and fluorescence of 7J/μm^2 was used.

The standard GEMOC GJ-1 zircon (TIMS normalisation data $^{207}Pb/^{206}Pb$ = 608.3Ma, $^{206}Pb/^{238}U$ = 600.7Ma and $^{207}Pb/^{235}U$ = 602.2Ma (Jackson et al., 2004)) was used. The accuracy of the GEMOC – GJ-1 zircon standard was tested with the second zircon standard, Plesovice (TIMS-ID U–Pb age: 337.1 ± 0.4 Ma) (Sláma et al., 2008). Over the course of a 2 weeks all zircons were analysed, with Plesovice age mean age values at 332.8±9.9 at 95% confidence, MSWD of 1.09 and probability = 0.28 for $^{207}Pb/^{206}Pb$ and 338.1±1.2 at 95% confidence, MSWD of 1.06 and probability of 0.33 for $^{206}Pb/^{238}U$.

Data reduction was undertaken using the program "GLITTER!" (Griffin et al., 2008). The Microsoft excel extension Isoplot version 3.0 (Ludwig, 2003) was used when calculating the weighted mean ages, mean square weighted deviation (MSWD), concordia plots. The data were presented on concordia plots showing all age data, and a

second plot containing data within 10% of the concordia. Kernel density plots were created using the program DensityPlotter (Vermeesch, 2012).

Whole rock Major Element and Trace Element Geochemistry

Samples collected from the field were cut using the rock saw, crushed down to pebble sized particles using the jaw crusher then pulverised using the tungsten ring mill. From of each sample 4grams were measured out and heated overnight at to remove any water in the sample. The samples were mixed with meta-tetraborate flux at a ratio of 1:4 (sample to flux) to reduce their melting temperature, then once again heated over night again to remove any water from the sample. The samples were then melted down into fused disks which were sent to the CSIRO for XRF analysis.

The fused disks were then analysed on the NewWave 213 nm Nd-YAG laser in a He ablation atmosphere, coupled to an Agilent 7500cs ICP-MS at the University of Adelaide to obtain the trace element values. The standards NIST 610 (Gao et al., 2002), BCR-1 (Gladney et al., 1990) and BHVO-1 (Hollocher, 1995) were used to check the accuracy of the data. Data reduction was undertaken for using "GLITTER!" (Griffin et al., 2008). The spider diagrams are normalised to mid-ocean ridge basalts (MORB) using the standard diagram and normalising values of Pearce (1983), which was chosen on the basis of its wide use and objective approach (Rollinson, 1993; Rock, 1987). These spider diagrams along with the tectonic discrimination and rock classification diagrams were created using ioGAS.

Petrology

Samples that were collected from the field and representative sections of the rock were cut down to roughly 0.5 – 1cm in thickness and 10cm in length. These samples were

sent to Continental Instruments, Lucknow to be made into thin sections. The sections then were analysed via microscope under plain and cross polarized light to determine their mineralogy.

RESULTS

Petrology

A petrological analysis was undertaken in order to determine the mineral assemblage, any textures and features that may be evident in thin section. The following are the results of that analysis. Please note that mineral abundances will be able to be found in Table 1.

SH15-05 is a wholly crystalline, phaneritic, hypidiomorphic, coarse grained granite with large quartz, microcline, anorthite and plagioclase phenocrysts. Magnetite inclusions can be found within the biotite. This sample has the mineral assemblage of; magnetite, orthoclase, plagioclase, quartz, perthite and microcline.

The sample SH15-03 was found as an inclusion within SH15-05. It is a wholly crystalline, phaneritic, hypidiomorphic granite. All phenocrysts are similarly sized. Magnetite inclusions are present in the biotite. While this rock may have similar mineralogy as it's host, the abundances of each of the mineral are different, as can be seen in Table 1**.** This granite has the mineral assemblage of; biotite, orthoclase, plagioclase, microcline, quartz, magnetite and zircon.

SH15-02 is a wholly crystalline, phaneritic, hypidiomorphic monazite. There are large quartz, microcline, plagioclase and orthoclase grains. Plagioclase and Quartz ± orthoclase are seen breaking down to a highly birefringent mineral, which is likely is

muscovite. The mineral assemblage of this monazite is; biotite, magnetite, microcline, plagioclase, orthoclase, quartz, hornblende, muscovite and titanite

SH15-26 is a wholly crystalline, phaneritic, hypidiomorphic monazite. This sample has large microcline, quartz and plagioclase phenocrysts. A few isolated tourmaline needles can be found in the sample. Small zircon and magnetite grains can be found in the biotite of this sample. The mineral assemblage is; plagioclase, biotite, titanite, zircon, magnetite, tourmaline, microcline, orthoclase, quartz and hornblende.

The sample SH15-27 is a wholly crystalline, phaneritic, hypidiomorphic monazite. There are large grains of plagioclase, microcline and quartz. Commonly magnetite is found to be associated with biotite. Strangely there was no obvious orthoclase or hornblende in this sample. There appears to be very little mineral variability found in this sample. The mineral assemblage is; plagioclase, biotite, titanite, magnetite, microcline and quartz.

SH15-12 is a wholly crystalline, phaneritic, hypidiomorphic quartz monazite. There are large phenocrysts of microcline and quartz which dominate the sample. Only small quantities of plagioclase and clinopyroxene are present. Clinopyroxene seems to be breaking down to a feldspar which is possibly a sign of metamorphism. Relatively large, euhedral crystals of titanite are present, with their distinct diamond shape. The mineral assemblage is; titanite, biotite, zircon, magnetite, microcline, clinopyroxene, plagioclase and quartz

SH15-04 is a phaneritic granite with small finely grained and interlocking grains of microcline and quartz. This sample is dominated mostly by these microcline and quartz grains. Clinopyroxene is seen within many grains of plagioclase. The mineral

assemblage is; biotite, zircon, magnetite, microcline, clinopyroxene, plagioclase and quartz.

SH15-06 is a schist with a fine grained quartz/muscovite matrix and large porphyroblasts of Magnetite and Muscovite. Veins of fine grained tourmaline can be found throughout sections of the sample. The mineral assemblage of this sample is; chlorite, muscovite, quartz, magnetite, and tourmaline

SH15-14 is a porphyritic monzogabbro with fine grained quartz matrix and large porphyroblasts of fibrous to bladed chlorite. Sparsely dispersed throughout the rock are moderate to large grains of magnetite and clinopyroxene with small grains of biotite. The mineral assemblage is; biotite, magnetite, clinopyroxene, quartz and chlorite.

The sample SH15-16 is a porphyritic alkali gabbro with fine grained background mineral assemblage of biotite, hornblende and quartz. Large porphyroblasts of hornblende and chlorite are present with smaller magnetite grains throughout the sample. The mineral assemblage for this sample is; quartz, chlorite, biotite, magnetite and hornblende.

The granodiorite SH15-10 has two different textures. The first texture has large crystals of quartz, magnetite and biotite. The second texture has a fine grained quartz, muscovite and biotite matrix with large grains of biotite, magnetite and fibrous sillimanite. The mineral assemblage for this sample is; quartz, muscovite, biotite, magnetite and sillimanite

The alkalitic gabbro SH15-08 has two distinct crystal sizes; the background assemblage is needle like chlorite and quartz and the larger minerals consist of magnetite, chlorite, biotite and hornblende. The mineral assemblage for this sample is biotite, chlorite, hornblende, quartz and magnetite.

The sample SH15-09 is a granodiorite with large muscovite clusters in a matrix of interlocking, equally sized fine grained quartz, magnetic and biotite. The background assemblage forms an obvious flowing fabric is found between the muscovite clusters. The muscovite clusters appear as though they may be pseudomorphs of another mineral, however it was not possible to determine if this were true, or what that mineral may have been. Whilst the major element geochemistry of this sample identifies it as a granodiorite, it is obvious that this sample as undergone some measure of metamorphosis. The mineral assemblage for this sample is; muscovite, quartz, magnetite and biotite.

The sample SH15-26 is a wholly crystalline, phaneritic monazite with large interlocking minerals of roughly equal size. Zircon and magnetite are often found associated with biotite. The mineral assemblage of this mineral is; microcline, zircon, biotite, magnetite, plagioclase and quartz.

SH15-05		SH15-03		SH15-02	
Mineral	**Abundance**	**Minerals:**	**Abundances**	**Mineral**	**Abundance**
Biotite	10%	Biotite	30%	Biotite	10%
Magnetite	5%	Orthoclase	20%	Magnetite	3%
Orthoclase	15%	Plagioclase	20%	Microcline	15%
Plagioclase	10%	Microcline	10%	Plagioclase	15%
Quartz	40%	Quartz	15%	Orthoclase	15%
Perthite	5%	Magnetite	5%	Quartz	30%
Microcline	15%	Zircon	<1%	Hornblende	5%
				Muscovite	2%
				Titanite	5%
SH15-26		**SH15-27**		**SH15-12**	
Mineral	**Abundance**	**Mineral**	**Abundance**	**Mineral**	**Abundance**
Plagioclase	15%	Plagioclase	15%	Sphene	5%
Biotite	10%	Biotite	15%	Biotite	15%
Titanite	2%	Titanite	3%	Zircon	1%
Zircon	1%	Magnetite	7%	Magnetite	5%
Magnetite	5%	Microcline	30%	Microcline	30%
Tourmaline	2%	Quartz	30%	Clinopyroxene	4%
Microcline	25%			Plagioclase	10%
K-spar	10%			Quartz	30%
Quartz	25%				
Hornblende	5%				
SH15-04		**SH15-06**		**SH15-14**	
Mineral	**Abundance**	**Mineral**	**Abundance**	**Mineral**	**Abundance**
Biotite	15%	Chlorite	5%	Biotite	5%
Zircon	5%	Muscovite	20%	Magnetite	15%
Magnetite	5%	Quartz	30%	Clinopyroxene	10%
Microcline	25%	Magnetite	35%	Quartz	30%
Clinopyroxene	5%	Tourmaline	10%	Chlorite	40%
Plagioclase	10%				
Quartz	35%				
SH15-16		**1st SH15-10 texture**		**2nd SH15-10 texture**	
Mineral	**Abundance**	**Mineral**	**Abundance**	**Mineral**	**Abundance**
Quartz	15%	Quartz	60%	Quartz	30%
Chlorite	35%	Muscovite	10%	Muscovite	30%
Biotite	10%	Biotite	10%	Biotite	10%
Magnetite	5%	Magnetite	20%	Magnetite	10%
Hornblende	40%			Sillimanite	20%
SH15-08		**SH15-26**		**SH15-09**	
Mineral	**Abundance**	**Mineral**	**Abundance**	**Mineral**	**Abundance**
Biotite	10%	Microcline	30%	Muscovite	40%
Chlorite	50%	Zircon	>1%	Quartz	40%
Hornblende	15%	Biotite	15%	Magnetite	10%
Quartz	10%	Magnetite	5%	Biotite	10%
Magnetite	15%	Plagioclase	10%		
		Quartz	40%		

Table 1.Table of minerals found in petrological analysis and their relative abundances in percent.

U/Pb Geochronology

IGNEOUS SAMPLES

SH15-05

The U/Pb geochronology data for sample SH15-05 shows significant scatter, the majority of which is outside 10% of the concordia (Figure 1). This appears to be due to the grains containing to common lead, which can be seen in the spectrum results from Glitter. Of the data that are close to the concordia, there is a cluster of data between 500 – 550Ma. Within 10% of the concordia, 6 data points are present (Figure 2**)** which a

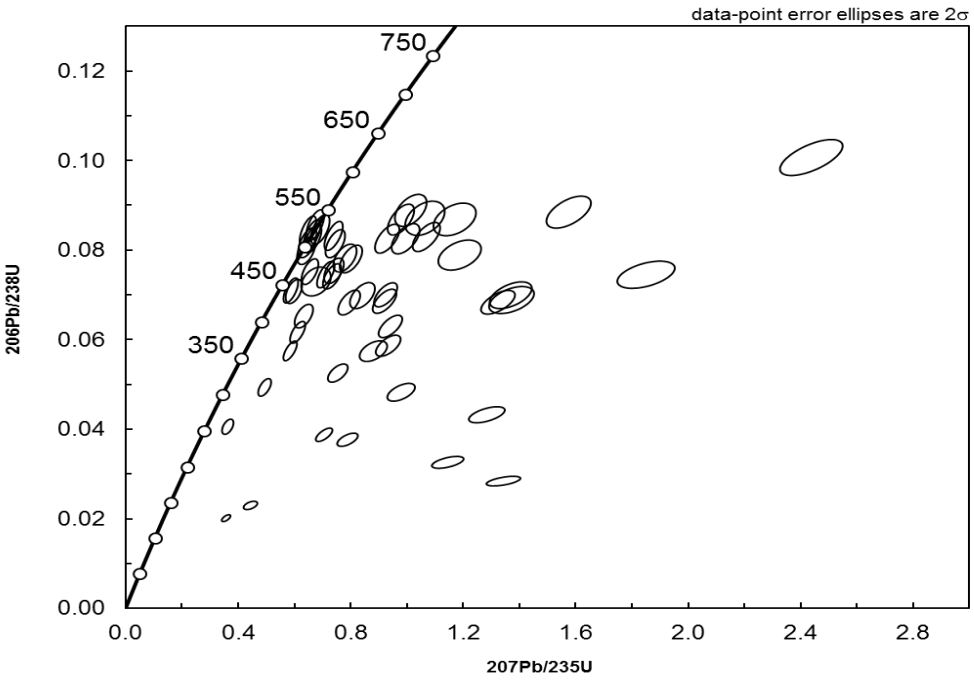

Figure 1. Concordia diagram of all age data from sample SH15-05.

cluster about ca. 490ma –ca. 550Ma. These give a mean $_{206}Pb/_{207}Pb$ age of 530±28Ma which is interpreted to be the best estimate of crystallisation due to its low MSWD.

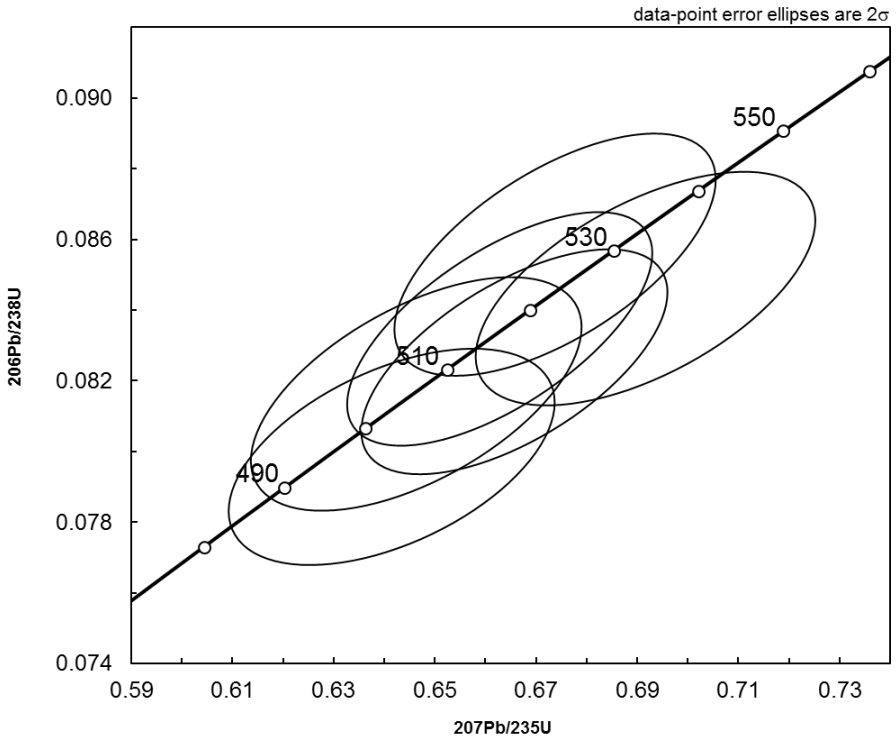

Figure 2. Concordia diagram of all age data within 10% of the concordia for sample SH15-05

SH15-26

The age data for SH15-26 yields ages between ca.470Ma to ca. 540Ma, with many data points laying away and below the concordia (Figure 3). Of these age data, the data that lie within 10% of the concordia shows a dense cluster of data around ca. 470Ma to ca. 540Ma (Figure 4). There are two significant outliers that skew much of the data, and therefore have been removed from these plots. These data give a mean Pb206-U238 age of 510.8±3.5 which is interpreted to be the best estimate of the age of crystallisation base on its low MSWD

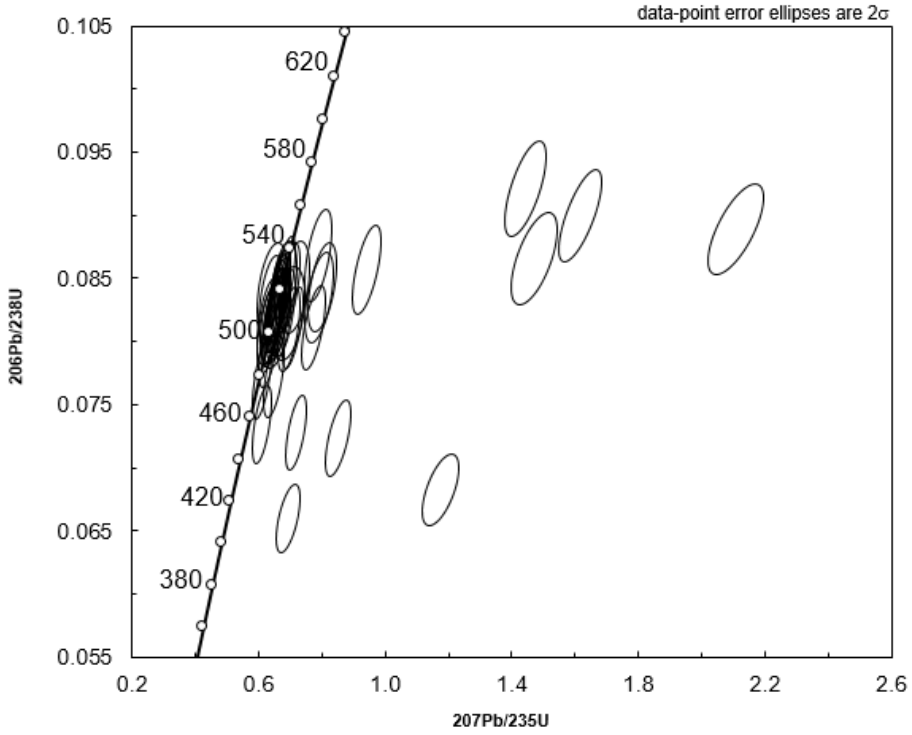

Figure 3. Concordia diagram of all age data from sample SH15-26

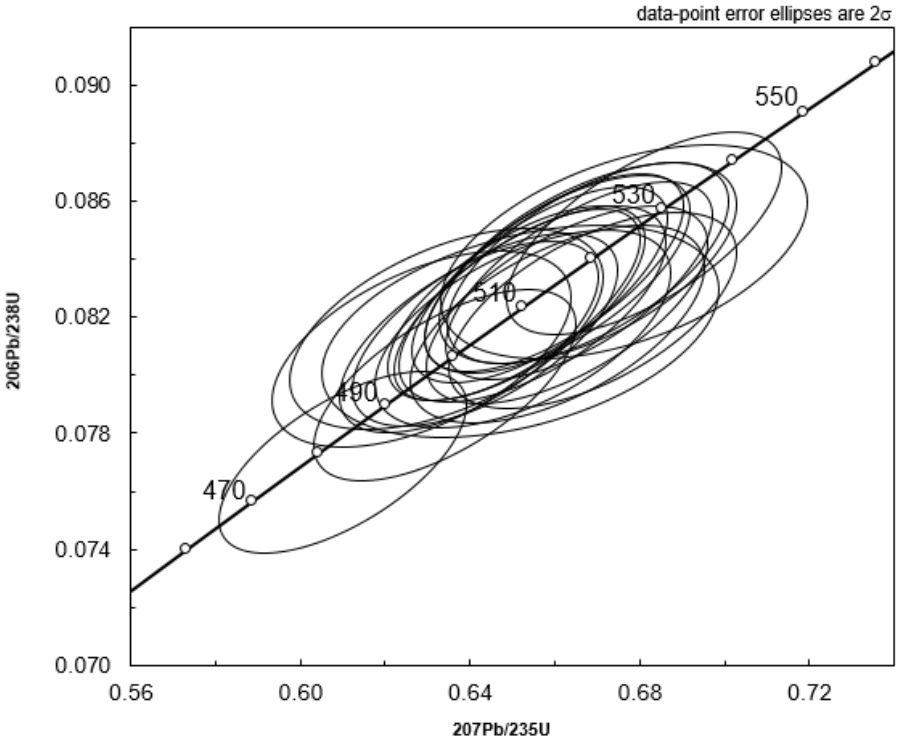

Figure 4. Concordia diagram of all age data within 10% of the concordia for sample SH15-26

SH15-12

U/Pb ages for SH15-12 have given data clustering consistently around ca. 450-550Ma, with few results far from the concordia **(**Figure 5**)**. A greater number of values cluster within 10% of the concordia than in SH15-12, and cluster about ca.480 – 540Ma **(**Figure 6**)**. U/Pb ages for these data show ages of Mean Pb207-Pb206 age of 522±19 which is interpreted to represent the best estimate for crystallisation based on its low MSWD.

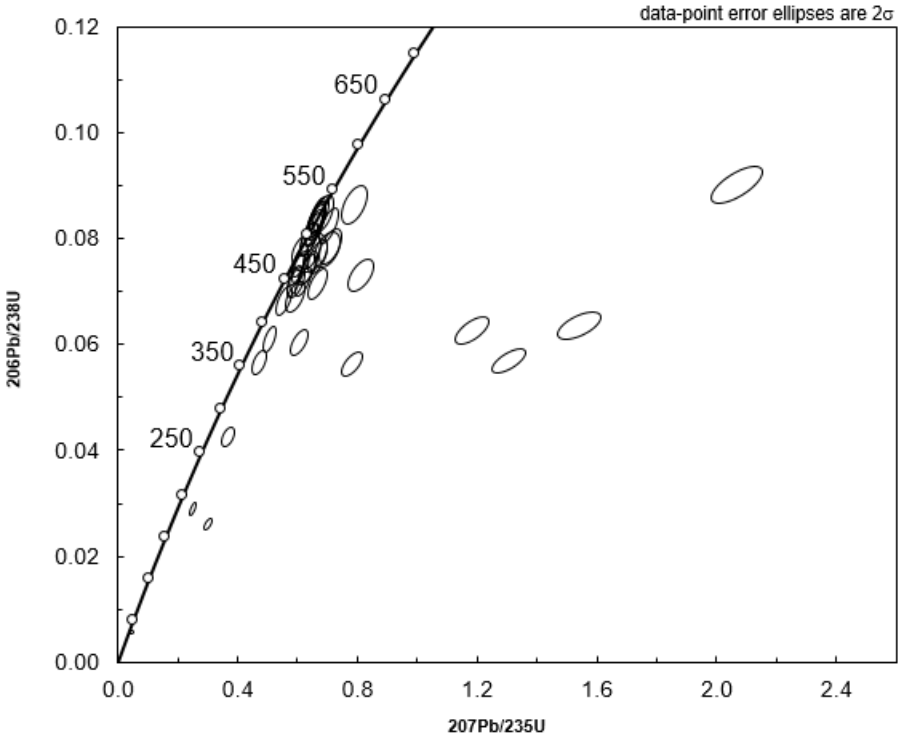

Figure 5. Concordia diagram of all age data for sample SH15-12

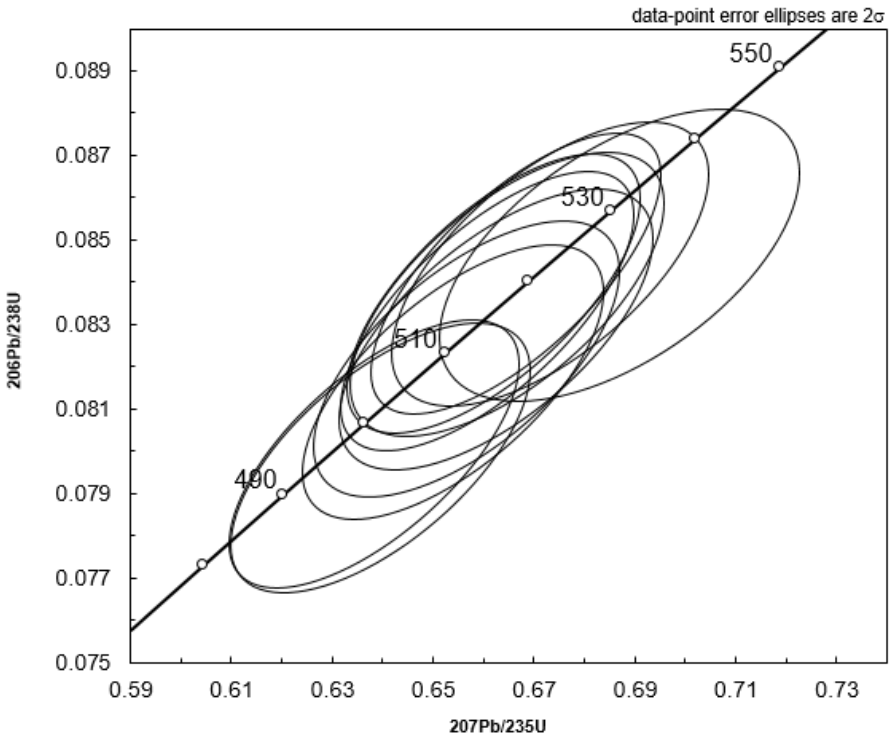

Figure 6. Concordia diagram for all age data within 10% of the concordia for sample SH15-12

SEDIMENTARY SAMPLES

SH15-21

Detrital zircons from sample SH15-21 yielded 85 analyses from which 66 zircons were within 10% of concordance (Figure 7; Figure 8). The main age peaks of these data are ca. 1750Ma, 2430Ma and 2530 Ma (Figure 9). These ages are interpreted to show the main detrital age components in the sample. The youngest near concordant zircon yielded a $_{207}$Pb-$_{207}$Pb age of 1131.4±28.29 Ma (102% concordant), which is interpreted as the maximum depositional age of the protolith to this rock.

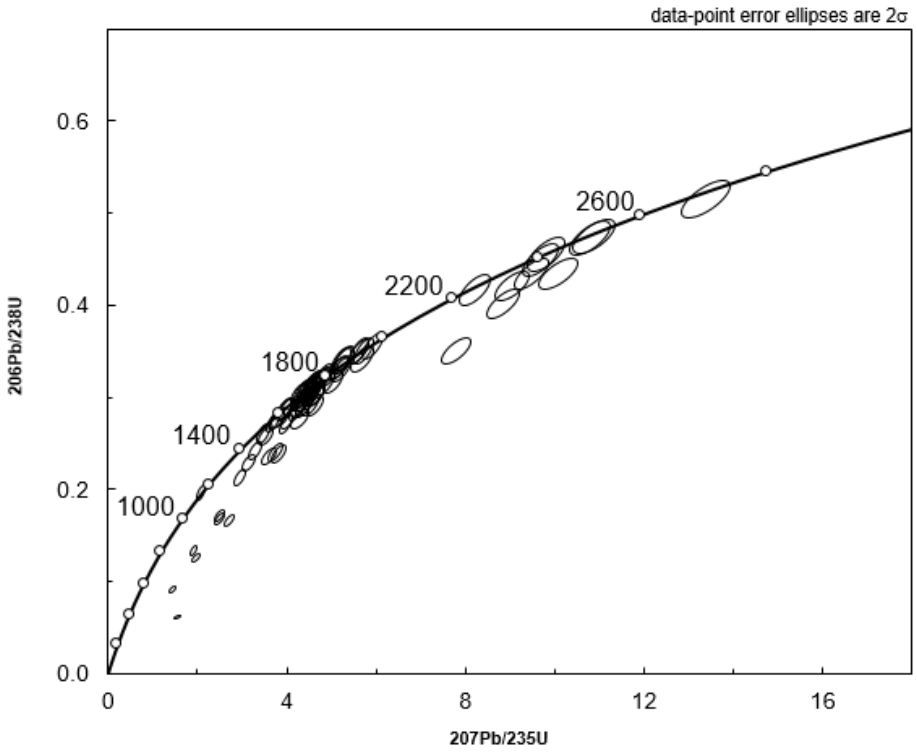

Figure 7. Concordia diagram of all age data for sample SH15-21

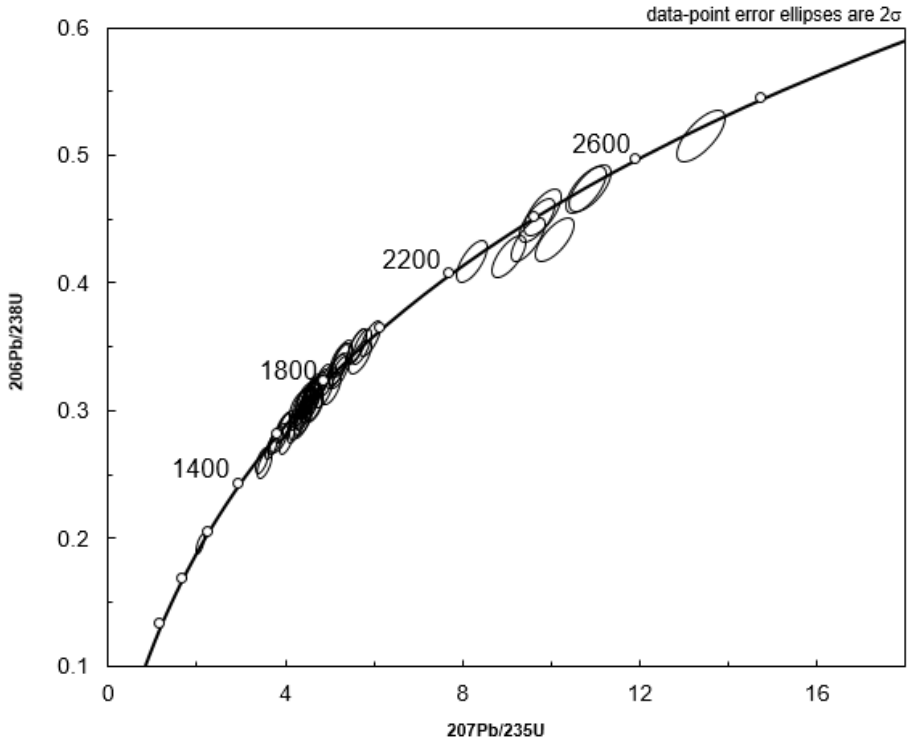

Figure 8. Concordia diagram of all age data within 10% of the concordia for sample SH15-21

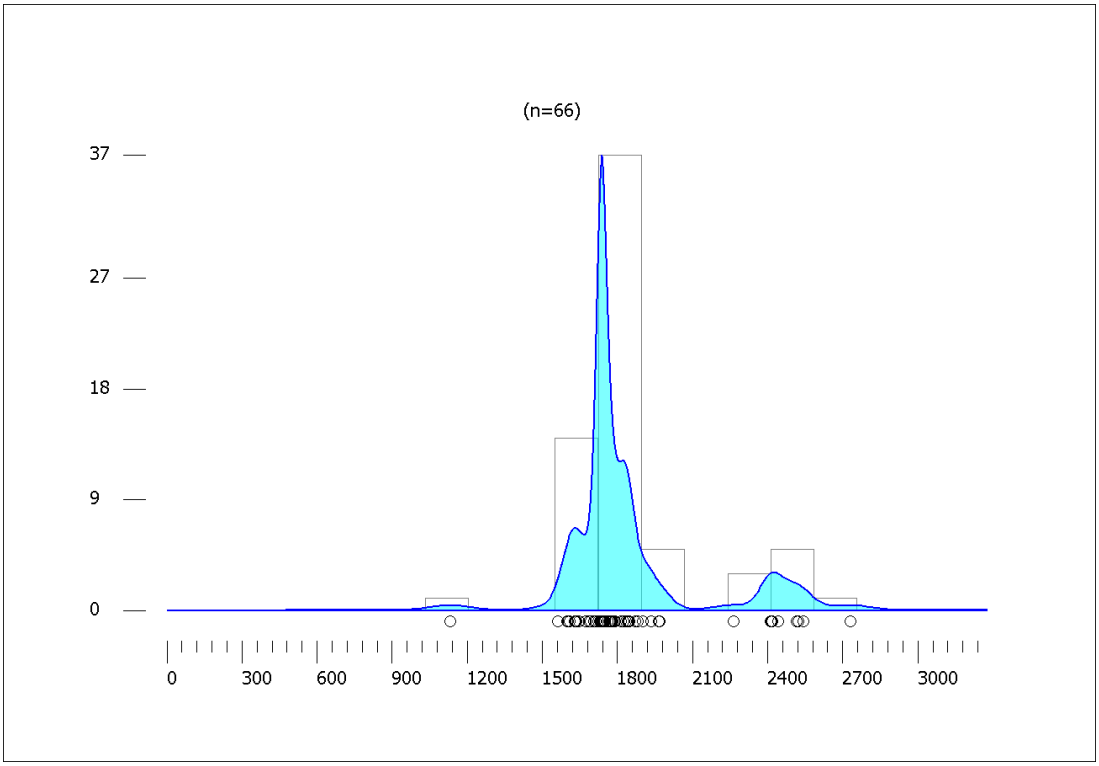

Figure 9. Concordia diagram for all $_{207}$Pb/$_{206}$Pb age data within 10% of the concordia for sample SH15-21

SH15-20

Sample SH15-20 yielded detrital zircon data from 77 analyses and 50 zircons that were within 10% of concordance **(**Figure 10**;** Figure 11**).** The dominate age peak in this data is ca. 1750Ma (Figure 12) and is interpreted to show the main detrital age components in the sample. The maximum depositional age of the protolith was determined using the youngest near concordant zircon, which yielded a $_{206}$Pb-$_{238}$U age of 1599.1±23.91Ma (94% concordant)

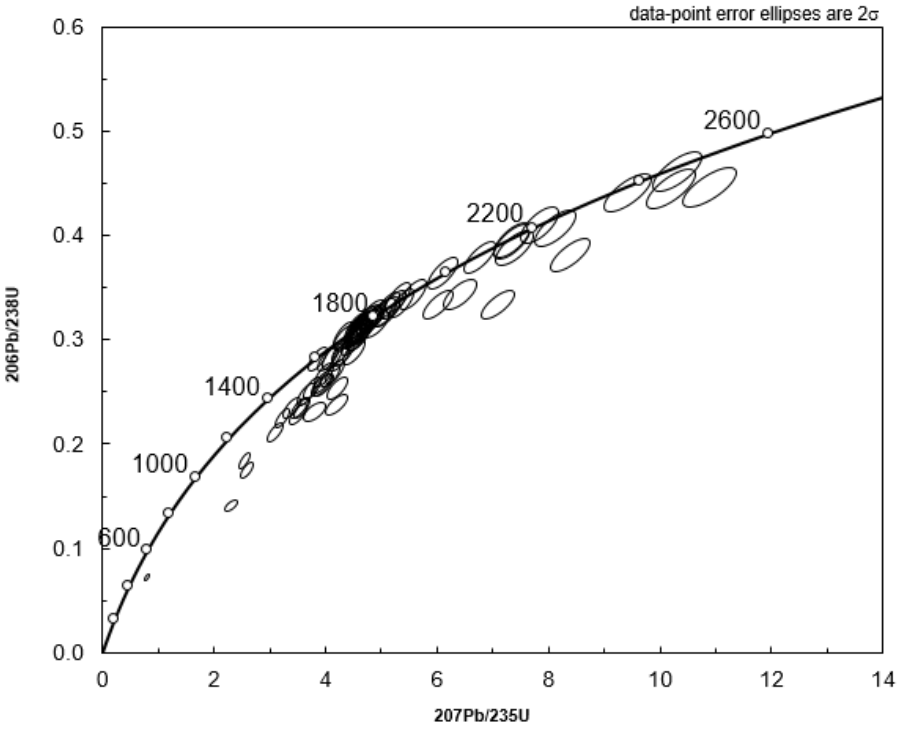

Figure 10. Concordia diagram of all age data for sample SH15-20

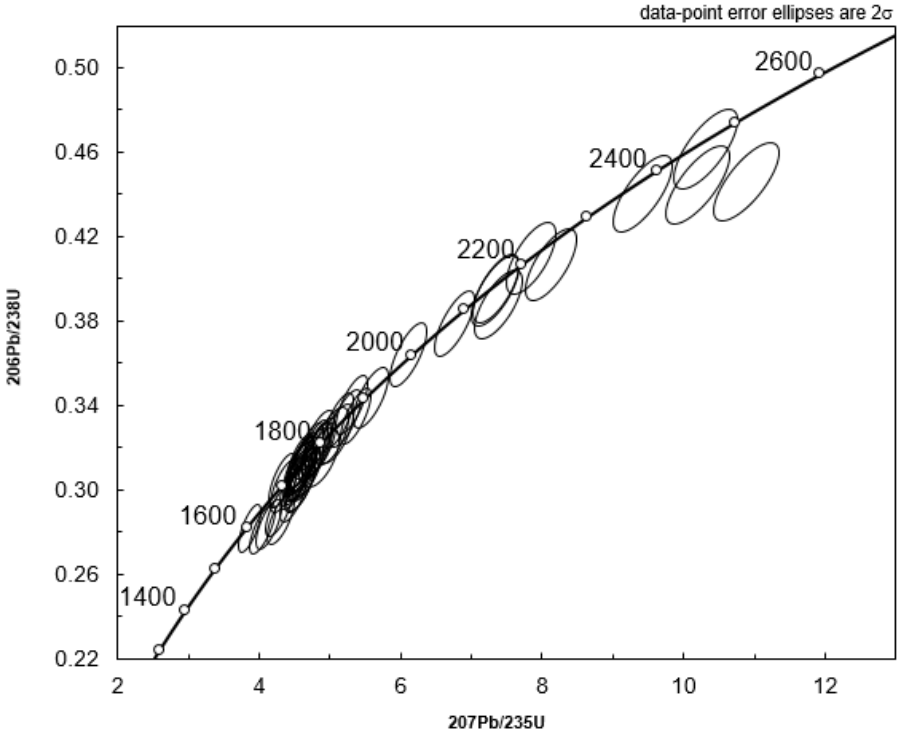

Figure 11. Concordia diagram of all age data within 10% of the concordia for sample SH15-20

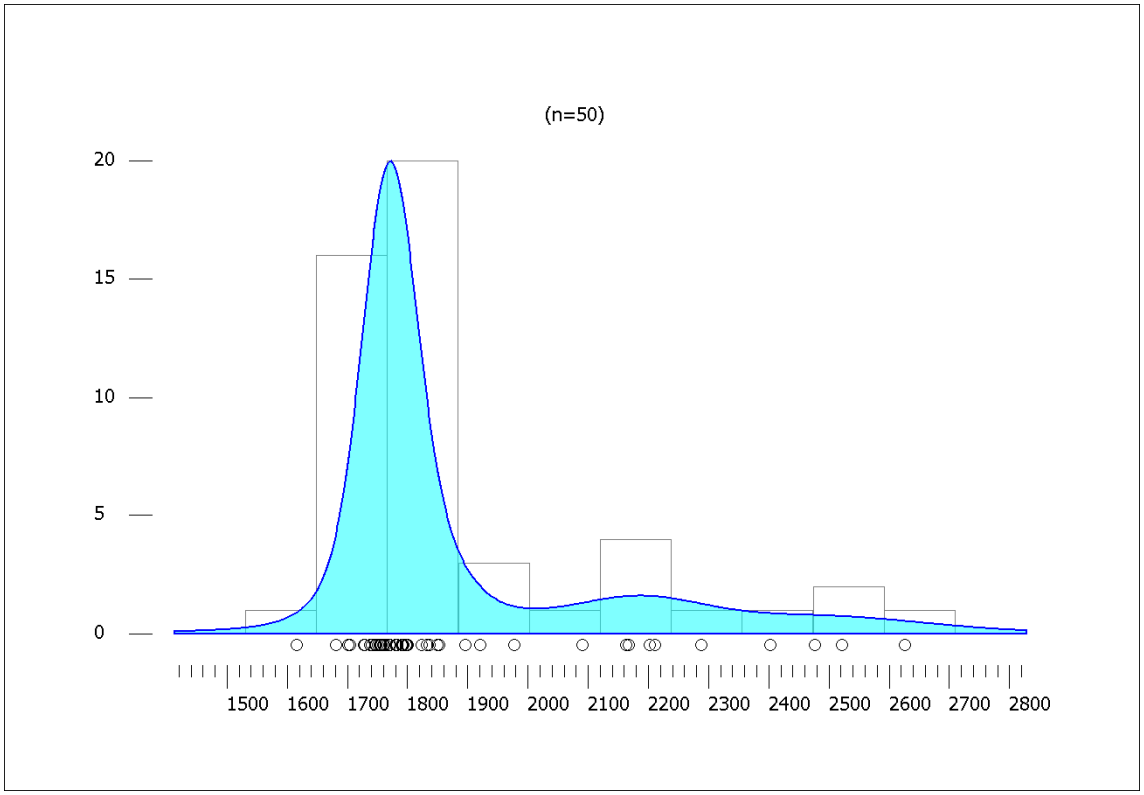

Figure 12. Kernel density plot of all $^{207}Pb/^{206}Pb$ age data within 10% of the concordia for sample SH15-20

SH15-19

Of the 69 analyses taken from sample SH15-19, 43 zircons that were within 10% of concordance (Figure 13; Figure 14). The majority of the age data peaked at ca. 1640 Ma and 1740Ma (Figure 15), which is interpreted to show the main detrital age components in the sample. A ^{206}Pb-^{238}U age of 1427.8±21.69Ma (90% concordant) was taken from the youngest near concordant zircon and interpreted to represent the maximum depositional age of the protolith of this rock.

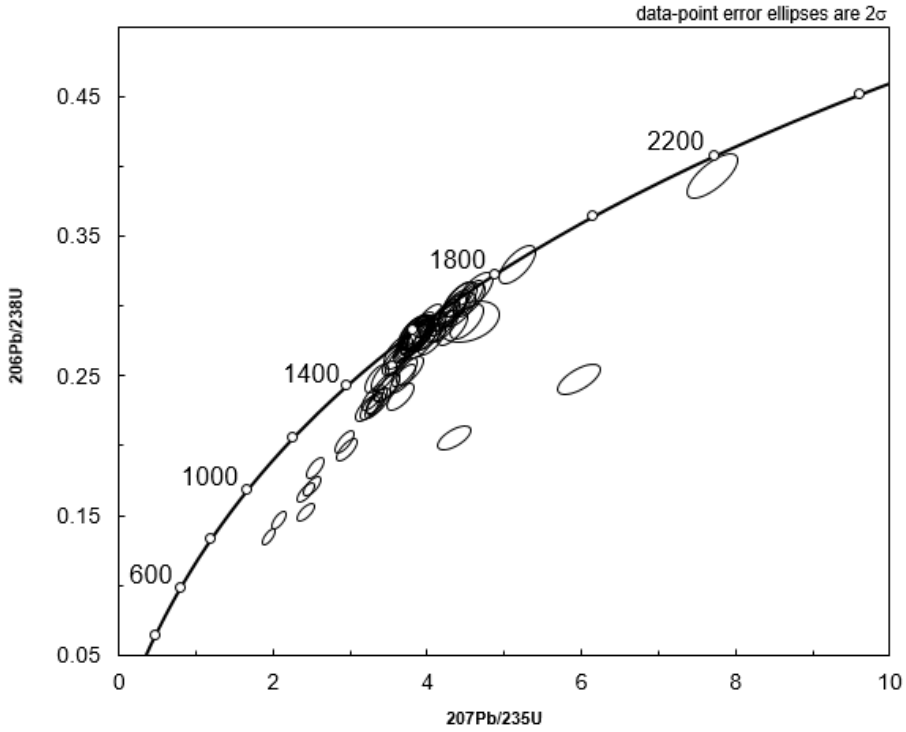

Figure 13. Concordia diagram of all age data for sample SH15-19

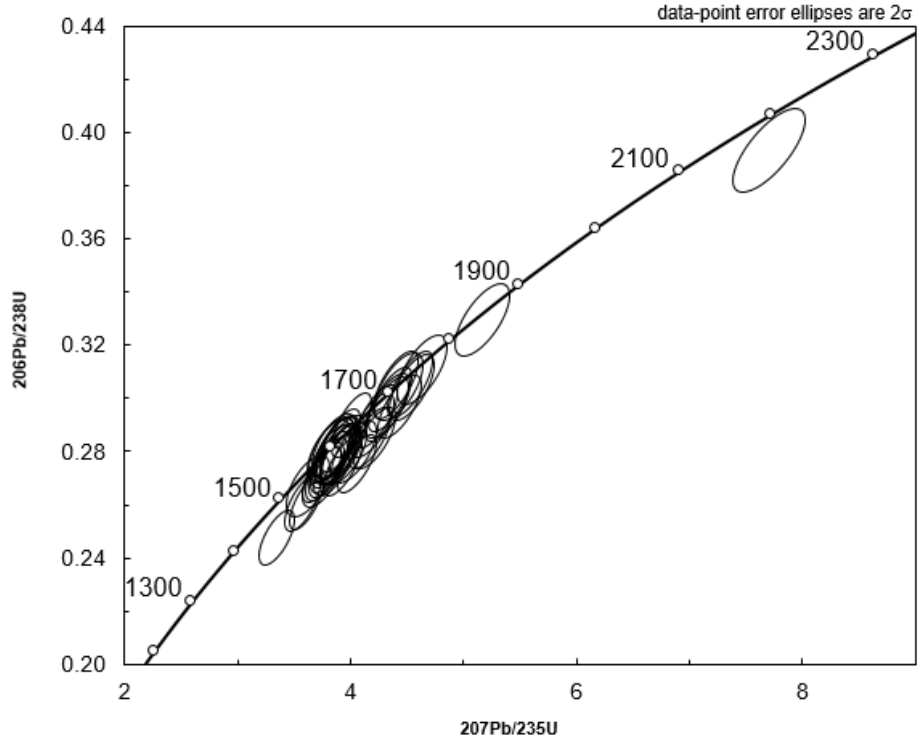

Figure 14. Concordia diagram of all age data within 10% of the concordia for sample SH15-19

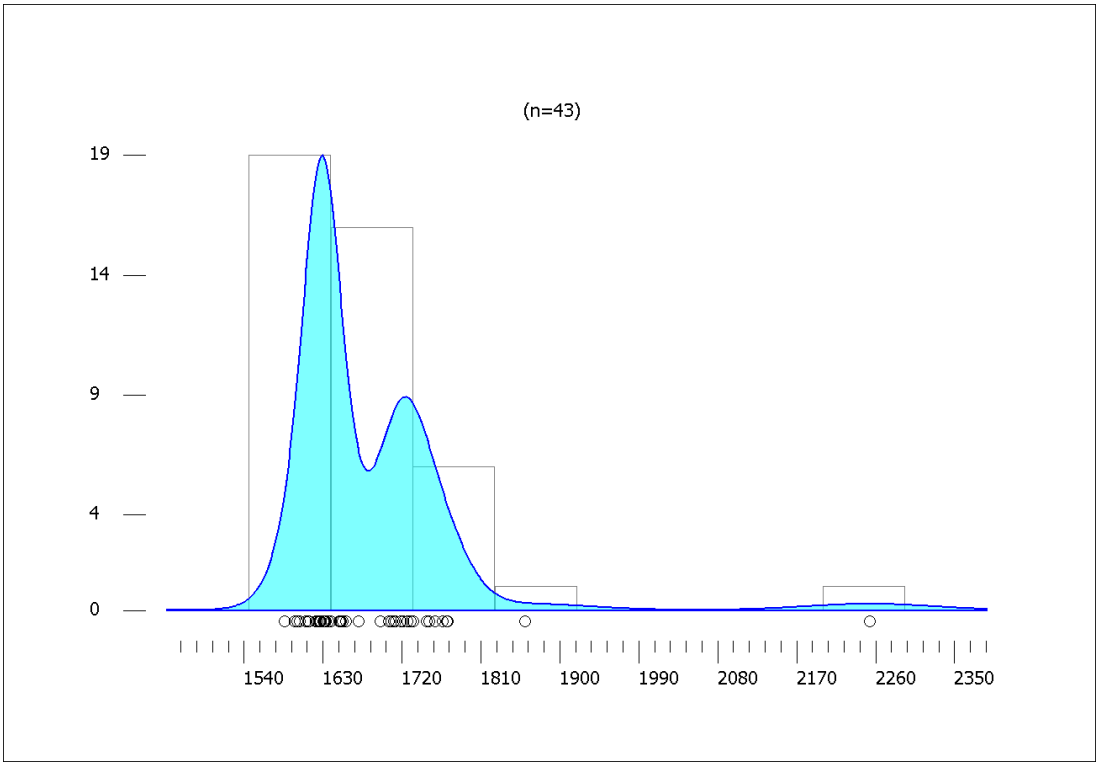

Figure 15. Kernel density plot of all $^{207}Pb/^{206}Pb$ age data within 10% of the concordia for sample SH15-19

SH15-18

There were 144 zircons within 10% of concordance for sample SH15-18 which were taken from 174 analyses (Figure 16; Figure 17). The main detrital age components in the sample were interpreted from the dominant age peaks at ca. 1180Ma, 1560Ma and 1780Ma (Figure 18). The youngest near concordant zircon was interpreted to represent the maximum depositional age of the protolith of this rock and yielded a ^{206}Pb-^{238}U age of 978.4±29.69Ma (105% concordant).

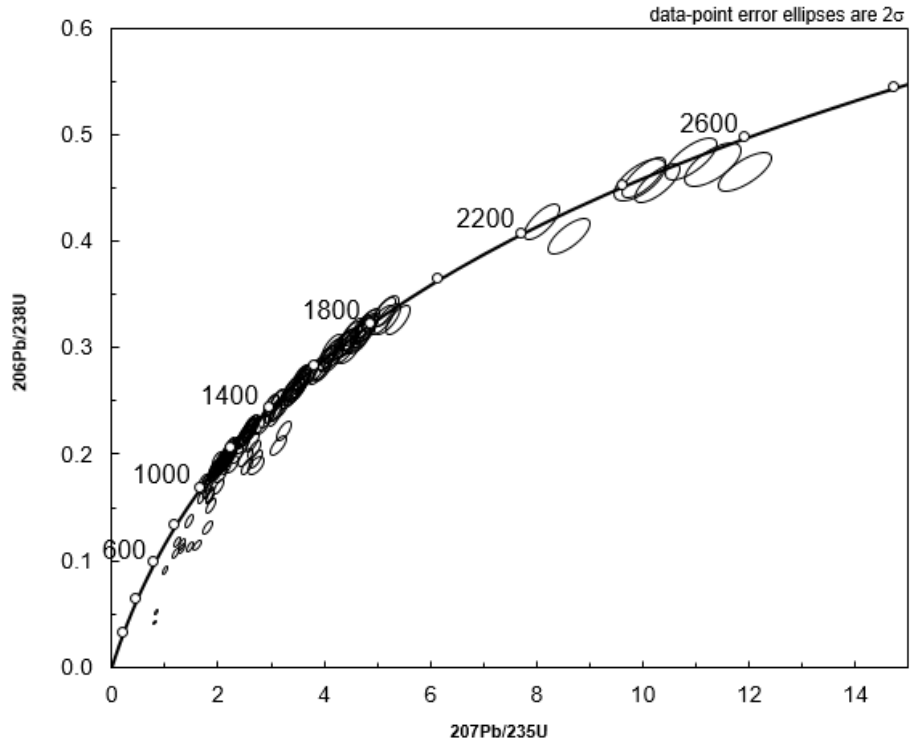

Figure 16. Concordia diagram of all age data for sample SH15-18

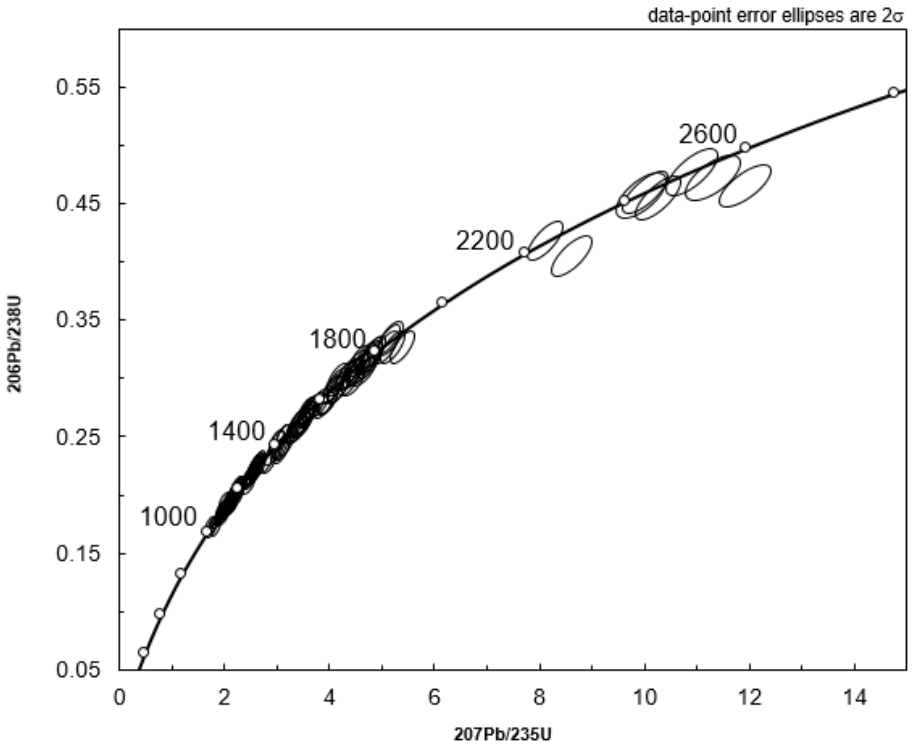

Figure 17. Concordia diagram of all age data within 10% of the concordia for sample SH15-18

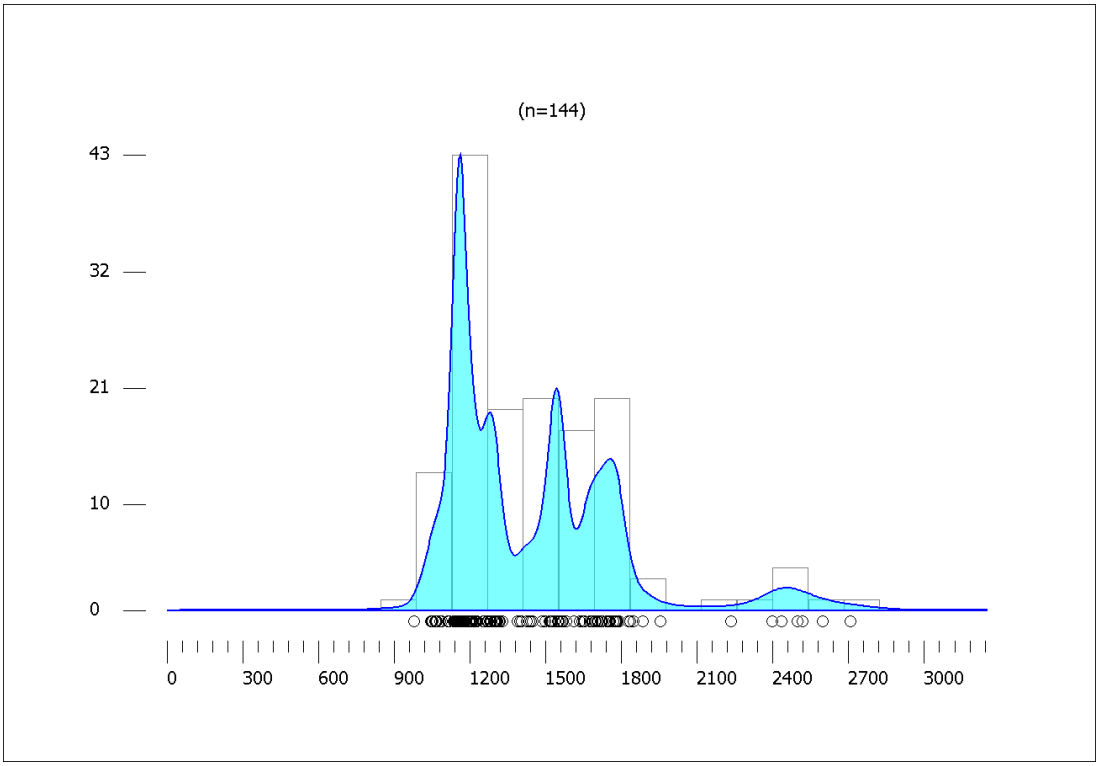

Figure 18. Kernel density plot of all $^{207}Pb/^{206}Pb$ age data within 10% of the concordia for sample SH15-18

Major element Geochemistry

FELSIC SAMPLES

SH15-05, 03 and 04 all share similar chemistry with Silica content ranging between 69.16% and 72.09% silica and 8.27% and 7.29% Na_2O+K_2O.On a total alkali vs silica (TAS)(Middlemost, 1994) plot (Figure 19), SH15-05 and 03 plot as granites, with due their silica and Na_2O+K_2O content. SH15-02, 26 and 27 have a silica content that ranges between 58.95% - 60.60% and total alkali content that ranges between 7.31% - 8.41%. This composition defines them as Monazites on a TAS (middlemost, 1994) plot. Samples SH15-09 and 10 have chemistry of 70.69% - 70.8% silica and 4.96% - 5.16% total alkali content making them plot on a TAS diagram (Middlemost, 1994) as

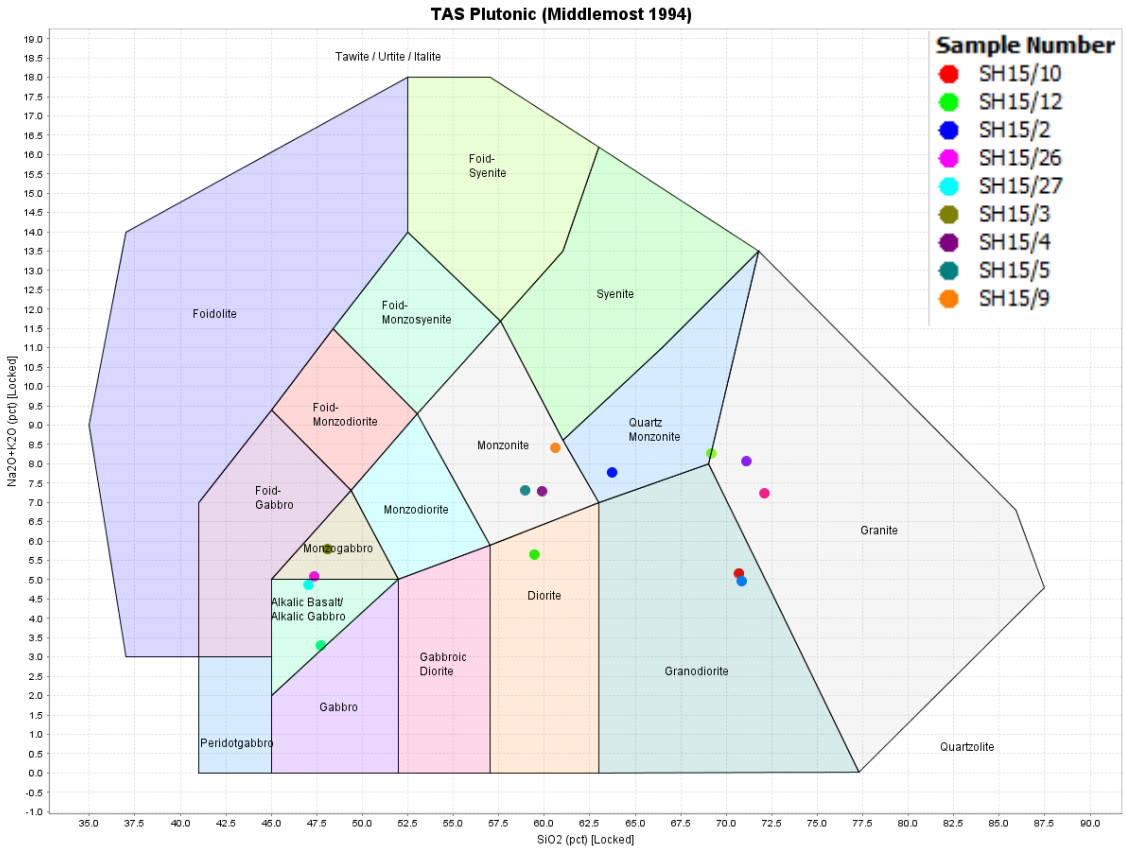

Figure 19. Total alkali silica (TAS) plutonic rock classification diagram containing all samples with major element geochemistry data.

granodiorite. SH15-12 has a silica content of 63.71% and total alkali content of 7.77%. On a TAS (Middlemost, 1994) diagram this defines the samples as a Quartz Monzonite.

Using the classification scheme set out by Frost et al., (2001) the major element data for the felsic samples have been classified according to their Fe Number (Figure 20), Modified alkali-lime index (MALI) (Figure 21) and Aluminium Saturation Index (ASI). Samples SH15-10, 3, 9 and 5 have been classified as Magnesian according to their Fe Number, Peraluminous by their ASI and calc-alkalitic by their MALI. The remaining samples were also classified using the aforementioned scheme. Samples 2, 27 and 26 were classified as Magnesian by their Fe Number, Alkalitic by their MALI and Peraluminous by their ASI. Sample 4 shares the same values for Fe Number and ASI, but with was classified by the MALI as alkali-calcic. The combination of these factors

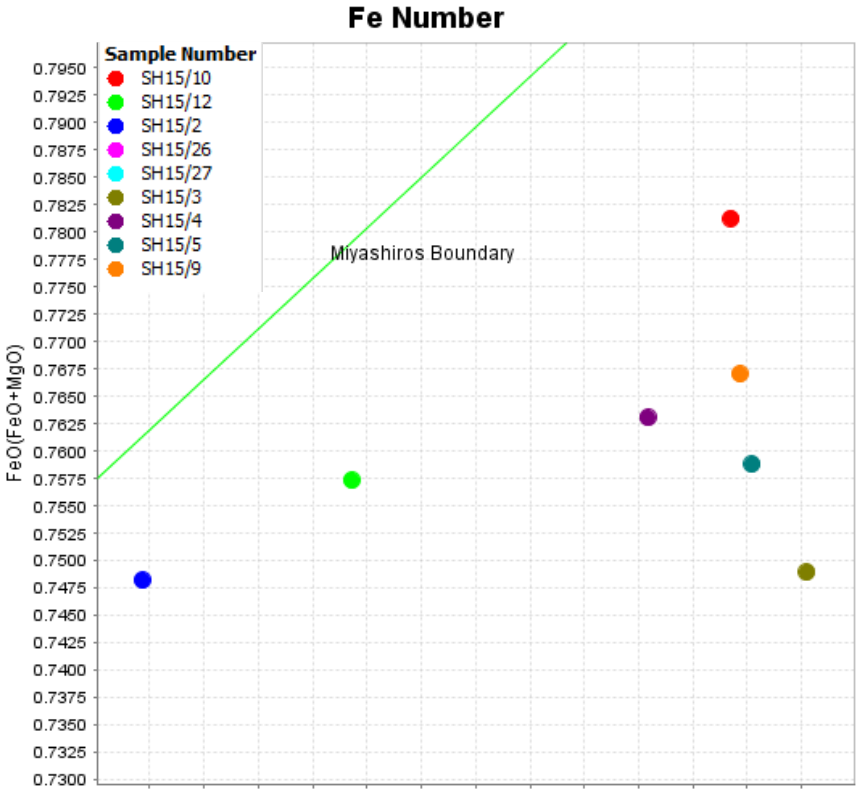

Figure 20. FeO/(FeO+MgO) vs SiO_2 diagram. The line, known as Miyashiros Boundary represents the boundary between ferroan and magnesian chemistry. The felsic samples all plot below the boundary, and therefore are magnesian.

makes these Cordilleran type granites, a set of granites classified by their calc-alkalitic chemistry and lack of Fe enrichment.

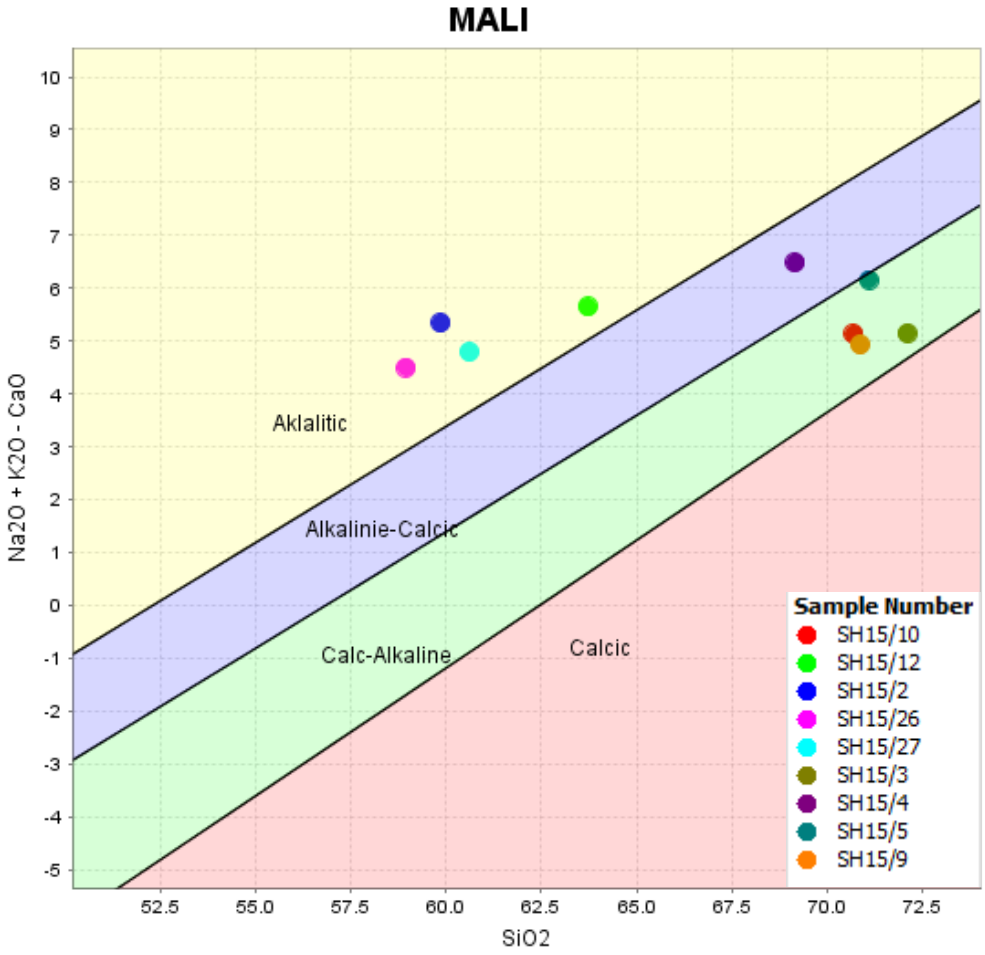

Figure 21. Na2O + K2O – Cao vs SiO2 diagram, otherwise known as a modified alkali-lime index (MALI) diagram. This diagram classifies samples based n how alkalitic to calcic they are. This diagram is used in the geochemical classification method created by Frost et al (2001)

MAFIC SAMPLES

Samples SH15-14 and 15 silica percentages of 47.36% – 48.10% and total alkali percentages of 5.08% - 5.78%. The two samples are defined as Monzogabbro on a TAS diagram (Middlemost, 1994) (Figure 19). SH15-16 has very similar chemistry to SH15-14 and 15, with a silica content of 47.02% and alkali content of 4.87%. On a TAS

diagram (Middlemost, 1994) the sample plots as an Alkali Gabbro. SH15-16 seems to be an intermediate between the composition of SH15-14 and 15 (Figure 19).

Trace Geochemistry

FELSIC SAMPLES

According to a Rb vs Y+Nb (Pearce et al., 1984) (Figure 22) SH15-12 and 10 are classified as coming from a syn-collisional tectonic setting. The Rb vs Y+Nb diagram defines SH15-26, 27, 03, 09 and 05 as granites originating from an island arc. This diagram also classifies SH15-4 as a within plate granite and SH15-02 as being from an orogenic setting, which may suggest that these samples may owe their orogen to an unrelated time and setting. Using a model by Brown et al., (1984) a Rb/Zr vs Nb

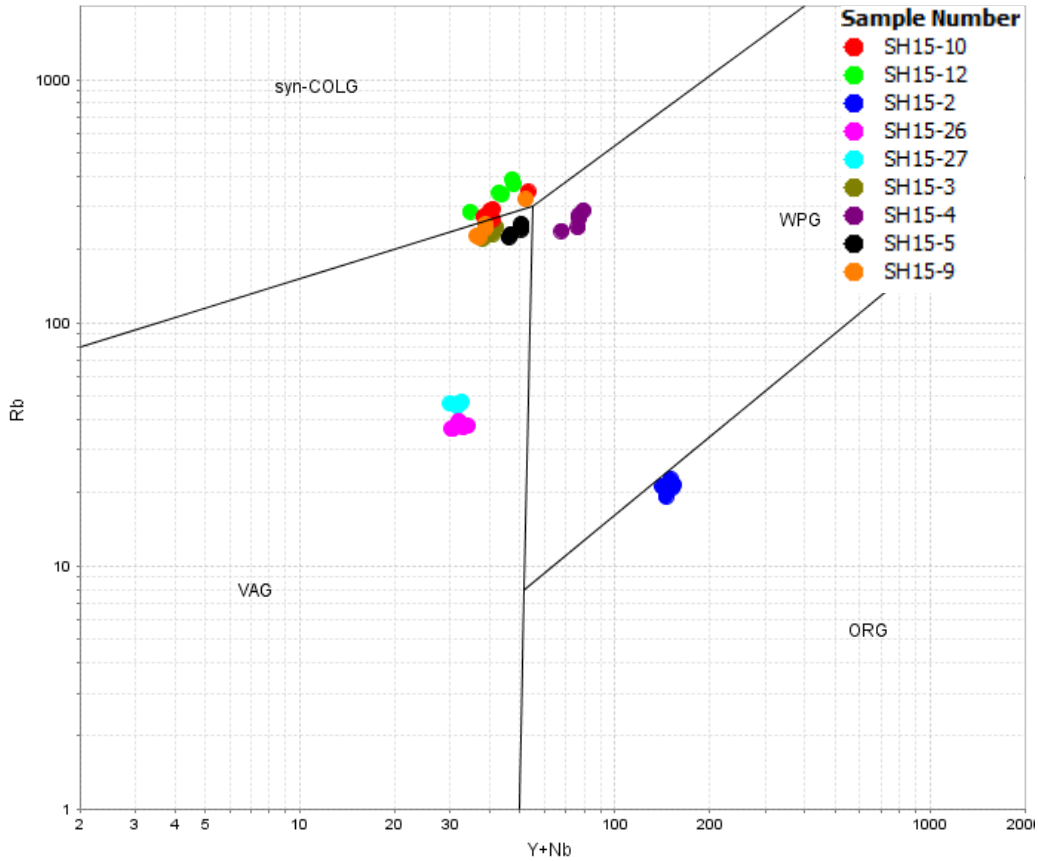

Figure 22: Rb vs Y+Nb diagram. This diagram by Pearce et al, (1984) discriminates the tectonic environments of the samples.

(Figure 23) diagram shows the how mature these granites are relative to each other, based on their enrichment in these elements. This plot shows that these granites mature in order of SH15-26, 27, 5 09, 10, 3 and then12 with SH15-12 being the most mature.

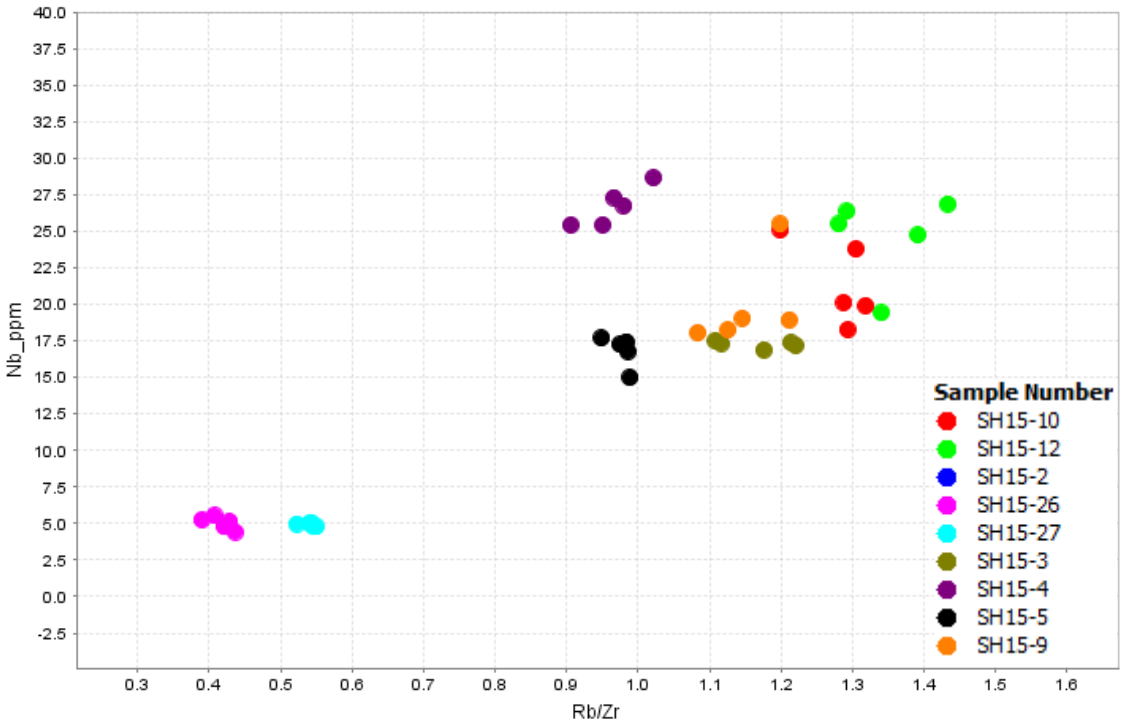

Figure 23: Nb vs Rb/Zr diagram. This diagram shows the maturity of magmatic arc granitoids. The enrichment of these elements has a positive relationship with the maturity of these granitoids, therefore the further towards the left of the diagram, the more mature the sample.

Using a normalised multi-element diagram, otherwise known as spider diagrams, further information can be taken from these data. The spider diagram of the felsic trace element data (Figure 24) shows enrichment of large-ion lithophile (LIL) elements with the exception of Sr, which is heavily depleted. Depletion of high field strength (HFS) elements relative to LIL elements can found within these data. In more detail, relative enrichment of Th and Rb is present, whilst there is relative depletion of Sr and TiO2. There are two distinctly different groups within these data while SH15-26 and 27 hold the similar pattern but the level of enrichment is lower relative all the other samples and they do not possess the same spike in the enrichment of Th.

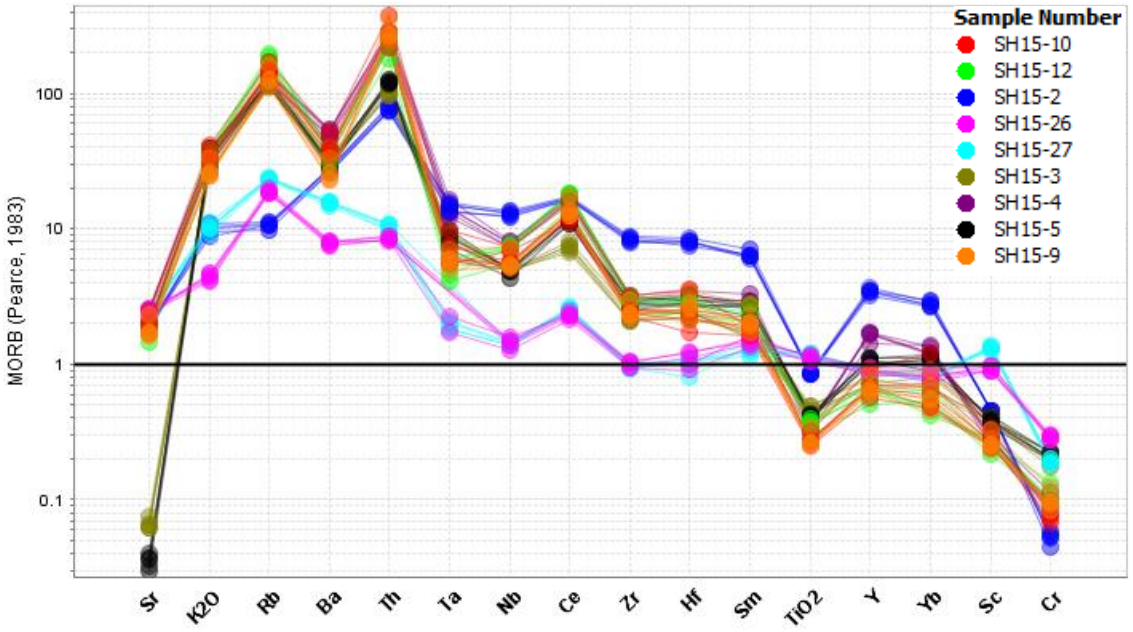

Figure 24. Spider diagram of felsic samples, normalised to MORB. This is the standard diagram and normalisation values of Pearce (1983).

MAFIC SAMPLES

A ternary plot of Th, Hf and Ta (Wood, 1980) (Figure 265), defines all of the samples as originating from a continental arc basalt (CAB) or volcanic arc basalt (VAB) settings. A spider diagram of the mafic trace elements (Figure 256) has been created in order to gain further information about the relative abundances and depletions found within these data. These data show relative enrichment of LIL elements, with relative depletion of HFS elements. In further detail, a spike in the enrichment of Ce is apparent, which is the exception to the rule of the relative depletion of HSF elements. Samples SH15-08, 11 and 15 follow the same trend at the same level, although SH15-11 has a depletion on Ba compared to the other two samples. Samples SH15-16 and 14 show the same overall trend of relative enrichment of LIL elements and depletion of HSF elements, although it displays an overall smoother trend.

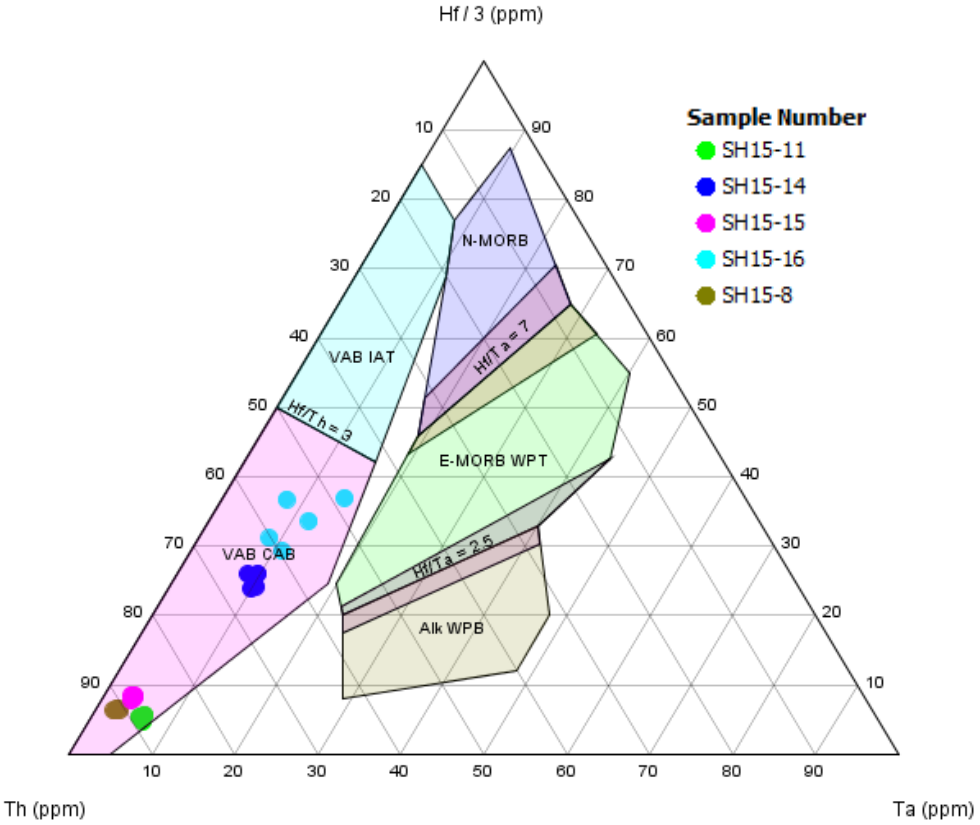

Figure 265. Hf/3 Th Ta ternary diagram (Wood, 1980)

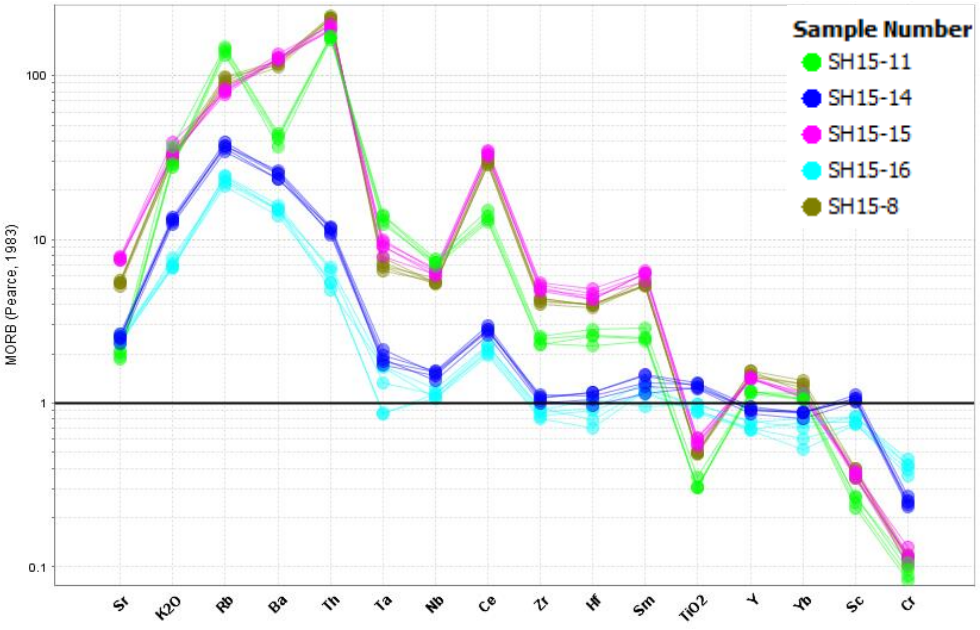

Figure 256. Spider diagram of mafic samples, normalised to MORB. This is the standard diagram and normalisation values of Pearce (1983).

DISCUSSION

Age Correlation

IGNEOUS

Using LA ICMPS U/Pb dating, ages of 530±28Ma, 530±28Ma and 522±19Ma were obtained, which correlate well with existing studies for the area. The igneous rocks dated by Yen et al., (2010) had shown ages of ca.520-430Ma from samples in the Shillong Plateau. Ghosh et al., (2005) got similar results from his study, with ages of ca.479MA and ca.550Ma from further west in the SMGC. While this study doesn't capture the range in ages that those papers did, they are all within the same similar period. These workers suggested that these rocks were created as a part of the amalgamation of Gondwana, as India collided with Australia along the Pinjarra Orogeny.

The ages found in this study also correlate well with the results of studies undertaken on other suggested regions attributed to the Pinjarra Orogen. Ages of ca. 570 -500Ma from Prydz Bay (Kelsey et al., 2008) ca. 515Ma from the Naturaliste Plateau (Halpin et al., 2008) and ca. 522Ma from The Leeuwin Complex (Collins, 2003) all correlate well with the ages produced in this study. Given the geochemical results, similar ages and position in Gondwana reconstructions, it can be suggested that the granitoids ages in this study may be a part of the Pinjarra Orogeny.

SEDIMENTARY

Using probability density plots the main populations within the detrital zircon data has been identified. Detrital zircon populations at were found at ca. 1150 and ca. 1180Ma, which compare nicely with the ages Yin et al., (2010) found, which range between ca.

900 and ca. 1250Ma. This is especially the case with SH15-18 which had its most common age at ca. 1180Ma. Yin et al., (2010) suggested that these ages correspond well with the crystallisation ages of the orthogneisses of the Mikir Hills, Shillong Plateau, and Brahmaputra River Valley. Given that the study Yin et al., (2010) undertook took place in the same area, is it reasonable to support their hypothesis.

It is important to note that while SH15-18 has a dominate age population around 1180, this is not the case for samples SH15-18, 19 and 20. These samples all had their most populous age at roughly 1750Ma. Yin et al., (2010) attributed these ages to the erosion of the crystalline basement which formed during the amalgamation of the two plates that collided to form proto-India. These ages could also be correlated with the gneisses found in Meghalaya, which ages at ca. 1700Ma (Ghosh et al., 1994), which Santosh and Rogers (2002) suggested may be the north eastern expression of the Central India Tectonic Zone. This is suggested by Santosh and Rogers (2002) to be the expression of the zone of compression that formed between Eastern India Western Australia during the completion of Columbia.

Tectonic environment

FELSIC SAMPLES

Major element geochemistry results were applied to a number of different classification systems to ascertain their chemistry and possible petrogenesis. Using the classification system set out by Frost et al., (2001) these samples all were classified as Peraluminous and Magnesian. The modified alkali-lime index (MALI) of these samples lend further insight into the samples setting, with samples SH-15 10, 3, 9, and 5 showing the calc-alkaline chemistry reflecting a position inboard of the batholithic belt. The remaining

samples SH-15 12, 2, 27 and 26 range in chemistry from alkali-calcic to alkalitic, reflecting that these samples lie even further inboard from the arc then the calc-alkaline samples, possibly as sparse plutons (Anderson and Cullers, 1990; John & Wooden 1990). Ghosh et al., (1991; 1994; 2005) who worked on many of the same rock reported similar finding, reporting the granites were calc-alkaline, I and S-type granites that varied between metaluminous to peraluminous.

The granitoids in this study can be compared to the Cordilleran batholiths of western USA and Mexico as a modern, better understood analogue of a magmatic arc. The batholiths of the Cordilleran batholithic belt are thought of as a magmatic arc, demonstrating magnesian, peraluminous to metaluminous and calcic to calc-alkaline chemistry (Frost et al., 2001). Further, previous workers have noted how the chemistry of these systems change from calcic to alkalitic as a function of distance from a postulated trench (Anderson and Cullers, 1990; John and Wooden, 1990). This observation can lead to further insights on the nature of this setting based on the modified alkali-lime index (MALI). Samples SH-15 10, 3, 9, and 5 show the calc-alkaline chemistry reflecting the intrusion occur either at or closely inboard of the batholithic belt. The remaining samples SH-15 12, 2, 27 and 26 range in chemistry from alkali-calcic to alkalitic, reflecting that these intrusions lie even further inboard from the arc then the calc-alkaline samples, possibly as sparse plutons (Anderson and Cullers, 1990; John & Wooden 1990).

Trace element data was plotted into a Y + Nb vs Rb (Pearce et al., 1984) (Figure 22) defining SH15-03, 05, 26, 9 and 27 as volcanic arc granites (VAG), which is in agreement with the major element results. Samples SH15-10 and 12 were classified as

syn-collisional granites, which in the case of SH15-12 is in agreement with the major element results and may explain the alkalitic chemistry of the sample. This doesn't explain the similar chemistry of SH15-10 to the VAG samples, although it should be said that SH15-10 stand very close to the boundary, so there may be a misclassification. The classification of SH15-02 and 04 as Orogenic (ORG) and within plate granites (WPG) respectively could be interpreted to either, 1) be representative of a totally different setting, either at the same or different time or 2) be supporting the hypothesis that the alkalitic chemistries of these granites reflects that they originate from further inboard of the suggested trench. It is unclear which of these hypotheses are correct, however without an U/Pb age for these samples a more conservative approach would suggest that these samples are from an unrelated event.

The spider diagram of the felsic samples in this study (Figure 24) show a relative enrichment of the LIL elements; K, Rb, Ba, and Th. These data also show a relative depletion of Ta, Nb, Ce, Zr and other HFS elements. This pattern of enrichment in LIL elements and depletion of HSF elements is indicative of a VAG (Deng et al 2012; Pearce 1996). These samples are all display a drastic depletion of Sr, which is likely due to Sr behaving as Ca and being incorporated into Calcium rich plagioclase and remaining in the magma source region.

A plot of Nb vs Rb/Zr (Browne et al 1984) (Figure 23) can be used to gain information about the maturity of the granites in a magmatic arc. This plot demonstrates the relationship between the samples chemistry, maturity and potentially, even tectonic environment. Combining the results from this diagram with the other results shows how if SH15-12 is ignored, there is a clear relationship between the maturity and how calcic

the samples are. Therefore, the more calcic the samples are, the more mature and the more inboard the plutons were located.

MAFIC SAMPLES

A spider diagram of these samples shows relative enrichment of the LIL Elements K, Rb, Ba and Th with the exception of Sr, which is relatively depleted in comparison to the other LIL elements. The HFS elements such as Ta, Nb, Zr and Hf show relative depletion, with the exception of Ce which is enriched. This pattern of LIL element enrichment and relative depletion of HFS is suggested to be indicative of an oceanic island basalts (OIB) (Sun, 1980).

A question that was intended to be answered by this study was whether the mafic and felsic samples intruded bimodally. Using a Th-Hf-Ta ternary diagram Wood, (1980) (Figure 26) all of the collected samples were found to plot as volcanic arc basalts (VAB). While no age data was collected from the mafic samples, the trace geochemistry results suggest the same tectonic environment as the felsic samples, originating in a magmatic arc. Based on the geochemistry results, it is suggested that these mafic samples intruded bi-modally, although, it must be acknowledged that without age data, it isn't possible to state this with a great deal of confidence.

Implications of study

Given the geochemical and geochronological results of this study, it can be suggested that the igneous samples used represent an island arc that formed somewhere around ca. 510Ma. This hypothesis fits well within the existing theories purposed for the India's role in the polyphase amalgamation of Gondwana. The calc-alkaline chemistries of these samples correlate well with the Collins and Pisarevsky (2005) observations, who

stated this is indicative of an island arc. Age data from these samples of 512.3±6.8 for SH15-12, 510.8±3.5 for SH15-26 and 513±13 for SH15-05 fit nicely within the Cambrian timeline purposed for the collision of the Indian plate with Australian/Mawson plate (Meert, 2003; Collins and Pisarevsky, 2005; Fitzsimons, 2000; Yin et al., 2010). These results also fit well into the model set out by Yin et al., (2010) who outlined a model of North Eastern India's geological history, where the subducting Australia/Mawson plate triggered arc magmatism within India between roughly 530Ma and 510Ma. With all this considered, it can therefore be suggested that the igneous samples detailed in this paper originate from that a magmatic arc generated by that event.

The detrital zircon ages gathered from the sediments of the Shillong Plateau, can be explained well with the hypotheses suggested by Santosh and Rogers (2002) and Yin et al., (2010). Age populations around 1750Ma to 1650Ma can be explained by the collision of the 2 plates that formed the proto-Indian continent. Santosh and Rogers (2002) suggest these times correspond with the collision of India and Antarctica during the amalgamation of Columbia. Ages of ca. 1100Ma to ca. 960Ma can be explained by arc magmatism during the collision of India and Antarctica along the Eastern Ghats-Rayner Orogen during the assembly of Rodinia (Yin et al., 2010; Santosh and Rogers, 2002). Given the crystallisation ages found in this detrital zircons, it can be suggested that these data support the hypotheses of Yin et al (2010) and Santosh and Rogers (2002).This would mean that these ages record two of India's ancient orogenic events, the amalgamation of Columbia and Rodinia.

CONCLUSIONS

Given their Magnesian, calc-alkaline to alkaline and peraluminous chemistry, it is suggested that the igneous samples analysed in this study originated in a magmatic arc. Adding to this, the relative enrichment of LIL elements and depletion of HFS elements can be used to further support this hypothesis. The plutonic system evolved over time, going from alkaline to calc-alkaline as it matured. Samples SH15-04, 12, 02, 27 and 26 intruded inboard of the subduction zone as a part of this earlier, more alkalitic stage. The system began intruding more calc-alkaline igneous bodies as it matured and intruded more outboard, towards the postulated trench, as is recorded by samples SH15-10, 03, 09 and 05. Using the chemistry of the mafic samples collected and analysed in this study, it is suggested that these bodies intruded bimodally with the felsic counterparts as magmatic arc basalts. The aforementioned igneous bodies intruded into the Shillong Group Sediments that are suggested to have been derived from orogenic events at around ca. 1750Ma in the formation of Columbia, and ca. 1150 and ca. 1180Ma in the formation of Rodinia. These igneous intrusions occurred at ca.510Ma, caused due to the subduction of the Australian/Mawson Plate underneath Greater India. The timing of these events lends further evidence to the theories of Meert (2003) and Collins and Pisarevsky (2005) amongst others that India collided with Gondwana during the Ediacaran to Cambrian, marking the completion of the super continent.

REFERENCES

Anderson J. L. & Cullers R. L. 1990. Middle to upper crustal plutonic construction of a magmatic arc; an example from the Whipple Mountains metamorphic core complex. *Geological Society of America Memoirs* **174**, 47-70.

Bilham R. & England P. 2001. Plateau /`pop-up/' in the great 1897 Assam earthquake. *Nature* **410**, 806-809.

Brown G., Thorpe R. & Webb P. 1984. The geochemical characteristics of granitoids in contrasting arcs and comments on magma sources. *Journal of the Geological Society* **141**, 413-426.

Collins A. S. 2003. Structure and age of the northern Leeuwin Complex, Western Australia: constraints from field mapping and U–Pb isotopic analysis. *Australian Journal of Earth Sciences* **50**, 585-599.

Collins A. S. & Pisarevsky S. A. 2005. Amalgamating eastern Gondwana: The evolution of the Circum-Indian Orogens. *Earth-Science Reviews* **71**, 229-270.

Deng J., Yang X., Sun W., Huang Y., Chi Y., Yu L. & Zhang Q. 2012. Petrology, geochemistry, and tectonic significance of Mesozoic shoshonitic volcanic rocks, Luzong volcanic basin, eastern China. *International Geology Review* **54**, 714-736.

Fitzsimons I. C. W. 2000. A review of tectonic events in the East Antarctic Shield and their implications for Gondwana and earlier supercontinents. *Journal of African Earth Sciences* **31**, 3-23.

Frost B. R., Barnes C. G., Collins W. J., Arculus R. J., Ellis D. J. & Frost C. D. 2001. A geochemical classification for granitic rocks. *Journal of petrology* **42**, 2033-2048.

Gao S., Liu X., Yuan H., Hattendorf B., Günther D., Chen L. & Hu S. 2002. Determination of forty two major and trace elements in USGS and NIST SRM glasses by laser ablation-inductively coupled plasma-mass spectrometry. *Geostandards Newsletter* **26**, 181-196.

Ghosh S., Chakraborty S., Bhalla J., Paul D., Sarkari A., Bishui P. & Gupta S. 1991. Geochronology and geochemistry of granite plutons from East Khasi Hills, Meghalaya. *Geological Society of India* **37**, 331-342.

Ghosh S., Fallick A. E., Paul D. K. & Potts P. J. 2005. Geochemistry and Origin of Neoproterozoic Granitoids of Meghalaya, Northeast India: Implications for Linkage with Amalgamation of Gondwana Supercontinent. *Gondwana Research* **8**, 421-432.

Ghosh S., Paul D., Bhalla J., Bishui P., Gupta S. & Chakraborty S. 1994. New Rb-Sr isotopic ages and geochemistry of granitoids from Meghalaya and their significance in middle-to late Proterozoic crustal evolution.

GLADNEY E. S., JONES E. A., NICKELL E. J. & ROELANDTS I. 1990. 1988 Compilation of Elemental Concentration Data for USGS Basalt BCR-1. *Geostandards Newsletter* **14**, 209-359.

Griffin W., Powell W., Pearson N. & O'Reilly S. 2008. GLITTER: data reduction software for laser ablation ICP-MS. *Laser Ablation-ICP-MS in the earth sciences. Mineralogical association of Canada short course series* **40**, 204-207.

Halpin J. A., Crawford A. J., Direen N. G., Coffin M. F., Forbes C. J. & Borissova I. 2008. Naturaliste Plateau, offshore Western Australia: A submarine window into Gondwana assembly and breakup. *Geology* **36**, 807-810.

HOLLOCHER K., FAKHRY A. & RUIZ J. 1995. TRACE ELEMENT DETERMINATIONS FOR USGS BASALT BHVO-1 AND NIST STANDARD REFERENCE MATERIALS 278, 688 AND 694 BY INDUCTIVELY COUPLED PLASMA-MASS SPECTROMETRY. *Geostandards Newsletter* **19**, 35-40.

Jackson S. E., Pearson N. J., Griffin W. L. & Belousova E. A. 2004. The application of laser ablation-inductively coupled plasma-mass spectrometry to in situ U–Pb zircon geochronology. *Chemical Geology* **211**, 47-69.

John B. E. & Wooden J. 1990. Petrology and geochemistry of the metaluminous to peraluminous Chemehuevi Mountains Plutonic Suite, southeastern California. *Geological Society of America Memoirs* **174**, 71-98.

Kayal J. R. 2008. *Microearthquake Seismology and Seismotectonics of South Asia* (Vol. 1). Springer, The Netherlands.

Kelsey D. E., Wade B. P., Collins A. S., Hand M., Sealing C. R. & Netting A. 2008. Discovery of a Neoproterozoic basin in the Prydz belt in East Antarctica and its implications for Gondwana assembly and ultrahigh temperature metamorphism. *Precambrian Research* **161**, 355-388.

Ludwig K. R. 2003. *User's manual for Isoplot 3.00: a geochronological toolkit for Microsoft Excel*. Kenneth R. Ludwig.

McWilliams M. O. 1981. Chapter 26 Palaeomagnetism and Precambrian Tectonic Evolution of Gondwana. *In:* Kröner A. ed., *Developments in Precambrian Geology*, Vol. Volume 4, pp 649-687, Elsevier.

Meert J. G. 2003. A synopsis of events related to the assembly of eastern Gondwana. *Tectonophysics* **362**, 1-40.

Middlemost E. A. 1994. Naming materials in the magma/igneous rock system. *Earth-Science Reviews* **37**, 215-224.

Nandy D. R. 2001. *Geodynamics of northeastern India and the adjoining region*. Acb Publ.

Payne J. L., Barovich K. M. & Hand M. 2006. Provenance of metasedimentary rocks in the northern Gawler Craton, Australia: Implications for Palaeoproterozoic reconstructions. *Precambrian Research* **148**, 275-291.

Pearce J. 1996. Sources and settings of granitic rocks. *Episodes* **19**, 120-125.

Pearce J. A. 1983. Role of the subcontinental lithosphere in magma genesis at active continental margins.

Pearce J. A., Harris N. B. & Tindle A. G. 1984. Trace element discrimination diagrams for the tectonic interpretation of granitic rocks. *Journal of petrology* **25**, 956-983.

Rock N. 1987. The need for standardization of normalized multi-element diagrams in geochemistry: a comment. *Geochemical Journal* **21**, 75-84.

Rogers J. J. & Santosh M. 2002. Configuration of Columbia, a Mesoproterozoic supercontinent. *Gondwana Research* **5**, 5-22.

Rollinson H. R. 2014. *Using geochemical data: evaluation, presentation, interpretation*. Routledge.

Sláma J., Košler J., Condon D. J., Crowley J. L., Gerdes A., Hanchar J. M., Horstwood M. S. A., Morris G. A., Nasdala L., Norberg N., Schaltegger U., Schoene B., Tubrett M. N. & Whitehouse M. J. 2008. Plešovice zircon — A new natural reference material for U–Pb and Hf isotopic microanalysis. *Chemical Geology* **249**, 1-35.

Sun S.-S. 1980. Lead isotopic study of young volcanic rocks from mid-ocean ridges, ocean islands and island arcs. *Philosophical Transactions of the Royal Society of London A: Mathematical, Physical and Engineering Sciences* **297**, 409-445.

Vermeesch P. 2012. On the visualisation of detrital age distributions. *Chemical Geology* **312**, 190-194.

Wood D. A. 1980. The application of a Th Hf Ta diagram to problems of tectonomagmatic classification and to establishing the nature of crustal contamination of basaltic lavas of the British Tertiary Volcanic Province. *Earth and planetary science letters* **50**, 11-30.

Yin A., Dubey C. S., Webb A. A. G., Kelty T. K., Grove M., Gehrels G. E. & Burgess W. P. 2010. Geologic correlation of the Himalayan orogen and Indian craton: Part 1. Structural geology, U-Pb zircon geochronology, and tectonic evolution of the Shillong Plateau and its neighboring regions in NE India. *Geological Society of America Bulletin* **122**, 336-359.